

ULTRAVIOLET SPECTRA OF THE CENTRAL STARS OF LARGE PLANETARY NEBULAE

JAMES B. KALER¹

Astronomy Department, University of Illinois

AND

WALTER A. FEIBELMAN¹

Laboratory for Astronomy and Solar Physics, NASA/Goddard Space Flight Center

Received 1982 August 6; accepted 1985 April 8

ABSTRACT

We have examined the ultraviolet spectra of 32 planetary nebula nuclei with the *International Ultraviolet Explorer*. Almost all the nebulae are quite large, with radii greater than 0.2 pc, and all are hot, with Zanstra temperatures $\geq 70,000$ K. In most cases, the fluxes at 1500 \AA are closely consistent with the visual magnitudes and the assumption of a hot blackbody. For some others, we provide improved m_v from an ultraviolet extrapolation, and in two instances (K1-14 and K1-22) new or alternative identifications of the correct central star. K1-16 may show variation, possibly related to that detected in the optical.

About half the stars exhibit a mixture of line features, most commonly He II $\lambda 1640$ and C IV $\lambda 1550$ in emission or absorption. Three display clear P Cygni lines: NGC 7094 at C IV $\lambda 1550$, Sp-1 at O V $\lambda 1371$ and N V $\lambda 1240$, and the well-known A78 at all three. A fourth, K1-16, appears to display a remarkably broad C IV $\lambda 1550$ P Cygni profile; if the identification is correct, the terminal velocity of the wind is about 8500 km s^{-1} . The ratio $v_\infty/v_{\text{escape}}$ may be ≥ 4 for these hot stars. The terminal velocity for Sp-1 is distinctly less than those of the others. The other half of the stars have no perceptible line features.

We analyze the continuous energy distributions through three flux-ratio indices, where we first employ the nominal, or standard, *IUE* calibration: $F(\lambda 1300)/F(\lambda 1750)$, $F(\lambda 1500)/F(\lambda 1850)$, and $F(\lambda 1500)/F(V = 5480 \text{ \AA})$. The distribution of these are fitted reasonably well both by the atmospheric models of Hummer and Mihalas and by blackbodies, with temperatures ranging from well under 10^5 K to infinity. We establish with some certainty that specific extreme stars have near-ultraviolet energy distributions indistinguishable from Rayleigh-Jeans, far too steep for the temperatures implied by the nebular spectrum. These extreme slopes indicate that models for very hot stars are in general inadequate. From the spectral indices, we calculate ultraviolet color temperatures (T_c) for comparison with Zanstra temperatures (T_z). Although the errors are large, we are clearly able to see that $T_c \gtrsim T_z$ (with T_c ranging up to, or near, infinity, as described above). The alternative *IUE* calibration adopted from the work of Finley, Basri, and Bowyer yields significantly lower (but often still quite high) slopes and temperatures, but appears to overcorrect, and we continue to adopt the standard calibration. Of the stars considered here, those with the Rayleigh-Jeans slopes tend to have the lower luminosities. The large, high-excitation nebulae, those with luminous nuclei for which the He II value of T_z is a lower limit, and which frequently have notable winds, have determinable (although sometimes very high) values of T_c . From the behavior of the lower luminosity stars, T_c is probably an upper limit for those of high luminosity, thus bracketing their true effective temperatures between T_z (He II) and T_c .

Subject headings: nebulae: planetary — spectrophotometry — stars: winds — ultraviolet: spectra

I. THE ULTRAVIOLET SURVEY OF CENTRAL STARS

Since the nuclei of planetary nebulae are among the hottest stars known, they are ideal candidates for observation in the satellite ultraviolet, $\lambda\lambda$ -1200–3300 \AA . A great deal of significant work can be done at optical wavelengths from the ground, including temperature and luminosity measurements by the Zanstra method, but in order to gain any complete understanding of these stars, it is imperative that we observe them in the UV, where the flux distributions begin to be sensitive to temperature, and where we can examine high-excitation line features. The importance of such studies can be seen in papers by Pottasch *et al.* (1978), Heap (1979), Greenstein (1981), Bohlin, Harrington, and Stecher (1982), Stecher *et al.* (1982), and many others.

¹ Guest observer with the *International Ultraviolet Explorer* satellite, which is sponsored and operated by the National Aeronautics and Space Administration, by the Science Research Council of the United Kingdom, and by the European Space Agency.

With this rationale, we set out to examine a significant number of planetary nuclei with the *International Ultraviolet Explorer* (*IUE*). So far, we have produced studies of two specific stars: see Feibelman and Kaler (1983) on the binary nucleus of LoTr-5, and Kaler and Feibelman (1984, hereafter KF1) on the effective temperature of Abell 78. In this our third paper, we survey all the data gathered to date and discuss significant statistical and general results. The details on the ultraviolet photometry of individual stars, or particular sets of stars, will be presented in later publications as full analyses are made, and as the supporting ground-based data are improved.

For our sample, we have chosen central stars primarily from the set of large planetaries observed by Kaler (1983a), for which the nebular radii are generally greater than 0.175 pc. Additional objects are NGC 7008, which at $r \approx 0.17$ pc is just under the above cutoff; nuclei of four other angularly large nebulae, IC5148-50, LoTr-5, Lo-1 = K1-26 (Longmore 1977; Kohoutek 1977); and K1-27 (Kouhoutek 1977). With some exceptions, we selected the brightest stars, generally those with

TABLE 1
JOURNAL OF OBSERVATIONS

Star (1)	PK (2)	Exposure ^a Number (3)	Date (4)	Exposure Time (minutes) (5)	Saturation Wavelengths (Å) (6)
NGC 246	118 - 74°1	SWP 14290*	1981 Jun 20	1.5	1225-1390
		LWR 10910*	1981 Jun 20	5	...
		SWP 18642*	1982 Oct 23	0.75	2450-2850
		LWR 14706	1982 Oct 23	2	...
NGC 2438	231 + 4°2	SWP 15501	1981 Nov 14	180	...
NGC 2474-2475	164 + 31°1	SWP 19397*	1983 Mar 5	120	1235-1375
NGC 2610	239 + 13°1	SWP 15502	1981 Nov 14	60	...
		LWR 11978	1981 Nov 14	85	...
NGC 6058	64 + 48°1	SWP 14293*	1981 Jun 20	10	1275-1325
		LWR 10913*	1981 Jun 20	20	...
NGC 7008	93 + 5°2	SWP 16898 ^b	1982 May 5	20	...
		LWR 13174 ^b	1982 May 5	28	...
NGC 7094	66 - 28°1	SWP 14289*	1981 Jun 20	12	1260-1290
		LWR 10909*	1981 Jun 20	30	2450-2925
IC 5148-5150	2 - 52°1	SWP 14213*	1981 Jun 7	120	1225-1425
		SWP 16968	1982 May 15	60	...
		SWP 17730	1982 Aug 21	60	1250-1300
A15	233 - 16°1	SWP 13524*	1981 Mar 17	90	1225-1390
		SWP 20276*	1983 Jun 20	35	...
A20	214 + 7°1	SWP 13525*	1981 Mar 17	130	1295-1315
A28	158 + 37°1	SWP 16965	1982 May 15	100	...
		SWP 19398	1983 Mar 5	70	...
A31	219 + 31°1	SWP 13526*	1981 Mar 17	60	1225-1375
		LWR 13237	1982 May 13	30	...
		SWP 16970*	1982 May 15	30	...
		SWP 18264*	1982 Oct 12	90	1225-1410
A33	238 + 34°1	SWP 14291*	1981 Jun 20	60	1225-1360
		LWR 13236*	1982 May 13	30	...
		SWP 16952	1982 May 13	30	...
A34	248 + 29°1	SWP 16951	1982 May 13	100	1225-1350
A36	318 + 41°1	SWP 14215*	1981 Jun 7	1.33	...
		LWR 10911	1981 Jun 20	4	2550-2860
A39	47 + 42°1	SWP 17237*	1982 Jun 16	40	...
A43	36 + 17°1	SWP 17733	1982 Aug 21	10	...
A51	17 - 10°1	SWP 13552*	1981 Mar 22	55	...
A65	17 - 21°1	SWP 18641*	1982 Oct 23	165	...
A72	59 - 18°1	SWP 14212*	1981 Jun 7	70	...
A78	81 - 14°1	SWP 13551*	1981 Mar 22	12	1225-1380
		LWR 10189	1981 Mar 22	30	2430-2975
		SWP 16966*	1982 May 15	6	...
		LWR 13250	1982 May 15	12	...
		SWP 19907	1983 May 5	4	...
		LWR 15881	1983 May 5	6	...
		SWP 19771	1983 Apr 20	25	...
A82	114 - 4°1	SWP 19908	1983 May 5	120	...
		SWP 15104*	1981 Sep 26	85	...
Jn-1	104 - 29°1	SWP 13549	1981 Mar 22	20	...
K1-14	45 + 24°1	SWP 13550*	1981 Mar 22	35	1225-1425
		LWR 13501	1982 Jun 16	35	2400-2900
		SWP 17235	1982 Jun 16	20	1225-1325
		SWP 18639	1982 Oct 23	10	...
		SWP 18640*	1982 Oct 23	60	...
		SWP 20271	1983 Jun 20	10	...
		SWP 20272	1983 Jun 20	10	...
		SWP 20273	1983 Jun 20	10	...
		SWP 20274	1983 Jun 20	10	...
		SWP 16969	1982 May 15	70	...
		SWP 21422*	1983 Oct 31	80	...
		SWP 17729	1982 Aug 21	80	...
		SWP 21421	1983 Oct 31	15	...
		Lo-1 ^e	255 - 59°1	SWP 16896	1982 May 5
SWP 16897	1982 May 5			10	...
LWR 13173	1982 May 5			20	2800-3125
SWP 17236	1982 Jun 16			10	...
LWR 13502	1982 Jun 16			10	...
SWP 19909	1983 May 5			5	...
LWR 15883	1983 May 5			5	...
SWP 17732	1982 Aug 21			60	...
SWP 18263*	1982 Oct 12			150	...
SWP 15102*	1981 Sep 26			65	...
Ym-29	205 + 14°1	SWP 15102*	1981 Sep 26	65	...

^a Asterisk marks exposure illustrated in Figs. 1-7.

^c Longmore 1977 = K1-26 (Kohoutek 1977).

^b No SWP image, weak LWR.

^f Longmore and Tritton 1980; see also Feibelman and Kaler 1983.

^d Kohoutek 1971.

^e Kohoutek 1977.

$V \lesssim 16$, and those with the lowest interstellar extinctions, in order to obtain the highest quality data. The observed stars cover a wide range in the $\log L$ - $\log T$ plane, $4.8 < \log T_z < 5.1$, and $0.9 < \log L_z/L_\odot < 3.7$, where T_z and L_z are He II Zanstra temperatures and luminosities (see Kaler 1983a). Most of the stars were too faint to be acquired directly by the satellite, or even to see on the FES acquisition camera, so that we had to work by blind offset from the nearest sufficiently bright star, the offset measured from the Palomar Sky Survey. The centerings, as indicated by geocoronal Lyman- α , are good for all exposures with the likely exceptions of A28 and Jn-1, and the possible exceptions A31 and Ym-29 (see § IVc[i]).

The observing log is presented in Table 1, where columns (1) and (2) list the common names and the Perek-Kohoutek (1967, hereafter PK) designations of the nebulae whose stars we have examined. Where the meaning is clear from the context, the stars and the nebulae will both generally be referred to by the nebular name.

All observations were made at low dispersion with the large aperture. Columns (3), (4), and (5) give the SWP or LWR exposure numbers, the dates of observation, and the exposure times in minutes. The last column shows wavelength regions of saturation, if any. All 32 stars were observed with the SWP camera, plus 11 with the LWR for which, because of the blackbody

nature of the star, the optimum exposure times are generally longer, and sometimes prohibitive. No image was recorded on the SWP exposure of NGC 7008, and only a weak one on the LWR, because of insufficient exposure due to interstellar extinction. Eleven stars were multiply observed with the SWP camera to provide optimum, or at least satisfactory, exposure times, especially to avoid saturation effects at the shortest wavelengths. We observed three multiply with the LWR camera. All data were reduced with the standard *IUE* programs, which produce useful and fairly accurate extrapolated fluxes in the saturated wavelength regions for the four remaining stars: NGC 2474-2475, 6058, and 7094 (SWP and LWR), and A34. The saturation problem is quite minor, except for the long-wavelength exposure of NGC 7094. Unless otherwise stated, we adopt the standard absolute flux calibration of Bohlin and Holm (1980). We discuss the general calibration problem in § IVd(iv).

Strong nebular line emissions are seen for NGC 2438, NGC 2610, and K3-27, which have high surface brightnesses relative to the others; we will report on these at a later time. About one-third of the exposures were reduced with extended rather than point extractions in order to see if weak emission could be detected around other stars: none was found. Several of these were reduced with point extractions for comparison. Except

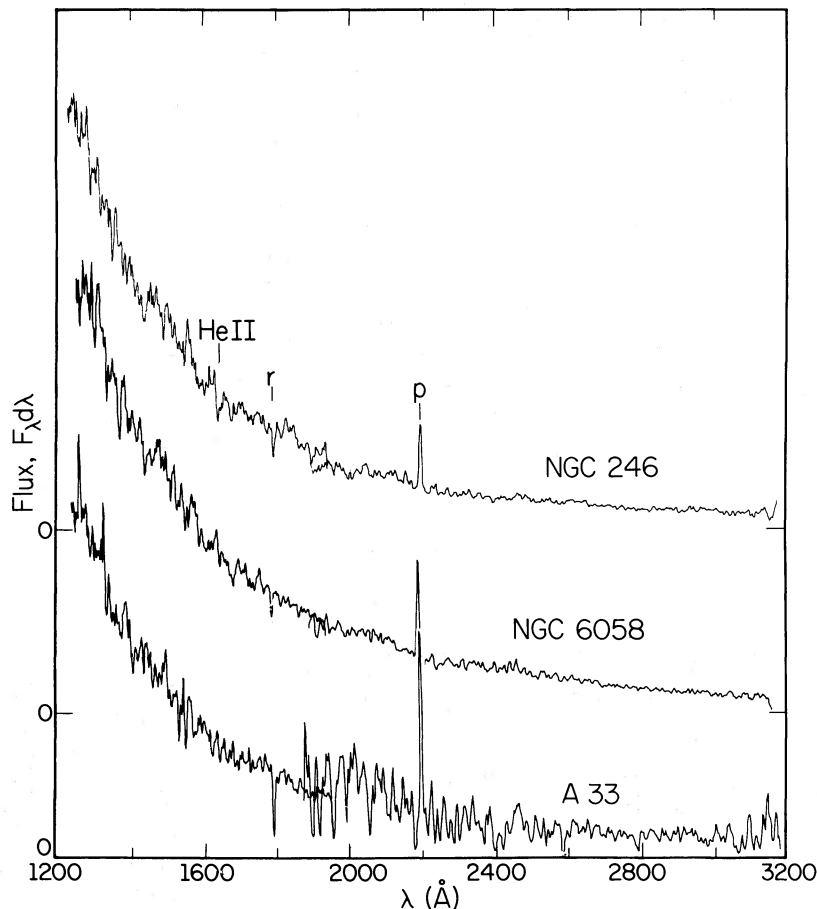


FIG. 1.—Full ultraviolet (LWR + SWP) spectra, uncorrected for reddening, of NGC 246 (SWP 18642), NGC 6058, and A 33, showing a realistic range in spectral quality. The zero points are indicated for each spectrum, as they are for later figures. The lower luminosity of the last star produces a noisier spectrum. The He II $\lambda 1640$ line is seen in NGC 246, and the interstellar 2200 Å feature is evident in NGC 6058. These are uncorrected for reddening, which is largest for A33. The letters *r* and *p* indicate a reseau mark and a bad pixel.

for a small increase in the noise for the faintest stars reduced with the extended source extractions, no systematic effects are found that distort the results of later sections.

The surface brightnesses of all nebulae except the above three are so low that nebular continuum is entirely insignificant. From Pottasch's (1984) calculations and Kaler's (1983a) data, K3-27 may be affected by as much as 10%. For the other two, evaluations are uncertain, since the observations were made in a central hole. NGC 2610 may be affected, and some caution is advised. For NGC 2438, the photowrite clearly exhibits background continuum superposed on the starlight longward of 1500 Å that may be due to the nebular continuum or to a field star. More detailed calculations can only be made when the line fluxes are reduced and analyzed.

We present samples of full spectra in the first three figures, which are designed to exhibit the range of the quality of the data. Figure 1 shows the full merged SWP and LWR spectra for two nuclei for which good data are available, NGC 246 and NGC 6058, and one for which we have moderate-to-poor

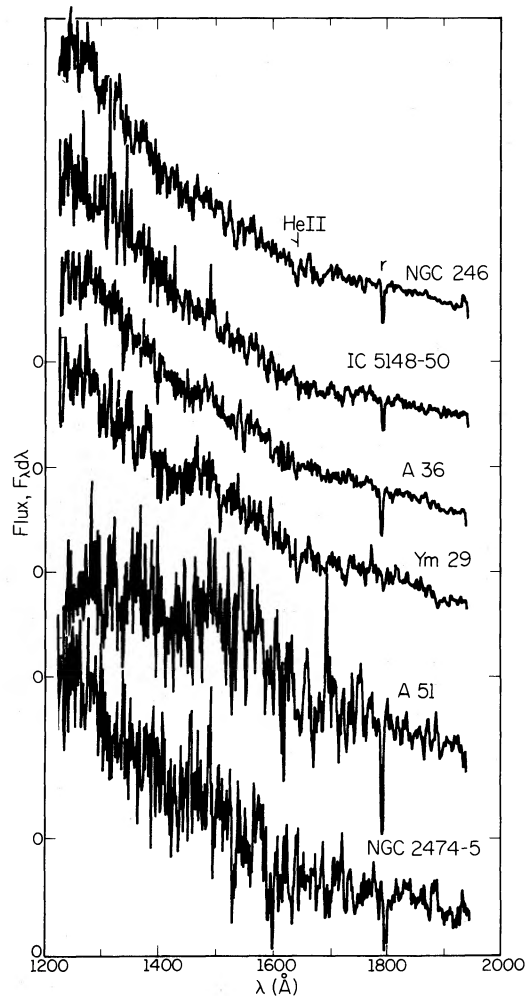


FIG. 2.—Shorter wave (SWP) ultraviolet spectra of NGC 246 (SWP 14290), IC 5148–50, A36, Ym-29 (=A21), A51, and NGC 2474–2475, selected in part again to exhibit the range in spectral quality. These are uncorrected for reddening, which is near zero for all but A51. Note the He II λ 1640 absorption in NGC 246 and Ym-29, and the 1470 Å break here and in Fig. 1. See Fig. 1 legend for further explanation.

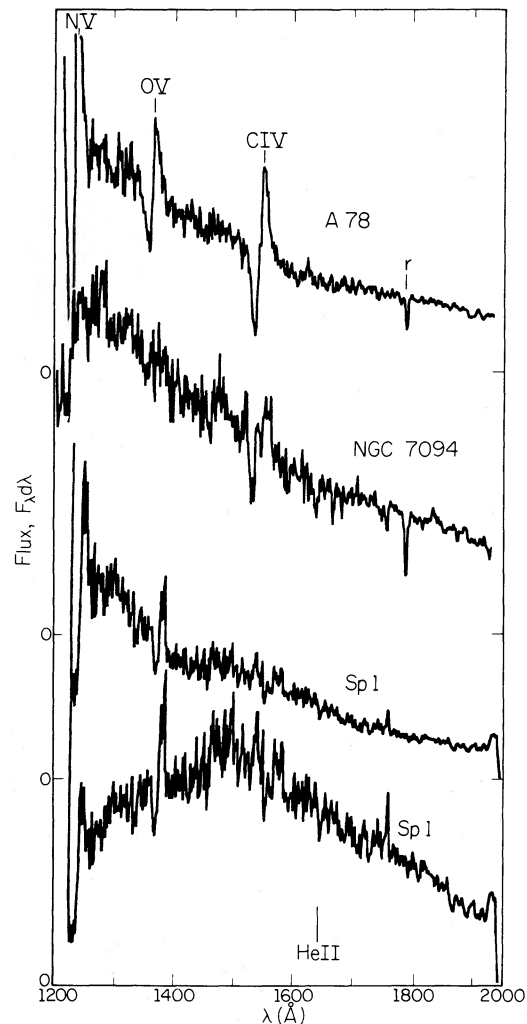


FIG. 3.—Full SWP spectra of three stars that display prominent P Cygni lines: A78 (SWP 13551), NGC 7094, and Sp-1 (SWP 18263). The first two are only lightly reddened and are uncorrected. Sp-1 is highly reddened, and both corrected (*upper*) and uncorrected spectra are presented. A78 shows lines of N v, O v, and C iv, and a possible line at 1310 Å (see KF1); NGC 7094 displays C iv, with He ii in absorption, and there is a very weak suggestion of O v; Sp-1 exhibits clear P Cygni profiles of N v and O v, with absorption at C iv and He ii. A78 and NGC 7094 also display the 2200 Å interstellar bump (not shown, see KF1). See Fig. 1 legend for further explanation.

observations, A33. Figure 2 exhibits SWP spectra of five more, IC 5148–5150, A36, Ym-29 (=A21), A51, and NGC 2474–2475, together with a second exposure of NGC 246. The first four are good low-noise exposures. The other pair is representative of the lesser quality data, with poorer signal-to-noise ratio, which result from exposures that are too short due to the faintness of the star, interference by Earth, or a high radiation background (many were taken during the US 2 shift). Figure 3 displays full SWP exposures for three stars that show P Cygni lines: A78, NGC 7094, and Sp-1. The latter is by far our most reddened object, and we plot it twice, as corrected for extinction (*above*), and as observed (*below*), to show the dramatic effect produced by interstellar dust. Aside from this one plot, all spectra are presented *as observed*, and are not corrected for reddening, as the extinction values are generally quite low.

TABLE 2
 SPECTRAL FEATURES

Star	λ (Å)	Identification ^a	Type ^a	W (Å)	N	Remarks
NGC 246	1640	He II	<i>a</i>	1.9 ± 0.4	2	C IV $\lambda 1550$ P Cygni (Heap 1982) not observed on this low- dispersion exposure uncertain
	2200	ISM	<i>a</i>	...	1	
NGC 2610	2200	ISM	<i>a</i>	...	1	
NGC 6058	2200	ISM	<i>a</i>	...	1	
NGC 7094	1371	O V	P	...	1	very uncertain
	1550	C IV	P	...	1	
	1640	He II	<i>a</i>	1.1:	1	somewhat uncertain
	2200	ISM	<i>a</i>	...	1	see KF1
	2511	He II	<i>a</i>	5.8	1	
A15	1550	C IV	<i>e</i>	3.5 ± 0.2	2	
	1640	He II	<i>e</i>	4.0 ± 1.4	2	
A20	1550	C IV	<i>e</i>	2.6:	1	uncertain
A31	1640	He II	<i>a</i>	1.7 ± 0.4	3	
A36	2200	ISM	<i>a</i>	...	1	
A39	1640	He II	<i>a</i>	2:	1	uncertain; artifact?
A65	1640	He II	<i>e</i>	1.7	1	uncertain
A72	1640	He II	<i>a</i>	0.6:	1	uncertain
A78	1240	N V	P	...	3	Heap 1979, KF1
	1310	Si II	P	...	2	KF1; uncertain
	1371	O V	P	...	3	Heap 1979, KF1
	1550	C IV	P	...	3	Heap 1979, KF1
	2200	ISM	<i>a</i>	...	3	KF1
	2734	He II	<i>a</i>	1.7	1	uncertain
Jn-1	1640	He II	<i>a</i>	2.9	1	
K1-16	1550	C IV	P	...	2	see text
	1640	He II	<i>a</i>	1.4 ± 0.1	2	
K1-27	1550	C IV	P	...	1	very uncertain
Lo-1	1640	He II	<i>a</i>	1.9	1	
Sp-1	1240	N V	P	...	1	
	1371	O V	P	...	1	
	1550	C IV	<i>a</i>	1.2:	1	uncertain
	1640	He II	<i>a</i>	1.3	1	
Ym-29	1640	He II	<i>a</i>	1.4	1	

^a ISM, interstellar; *a*, absorption; *e*, emission; P, P Cygni line.

II. SPECTRAL FEATURES

About half the stars have no detectable lines and exhibit only pure continua. Their lack may well be due only to insufficient signal-to-noise ratio; Heap (1982), for example, found the P Cygni profile of C IV $\lambda 1550$ in NGC 246 with high dispersion, but it is undetectable here with low. The features observed in the spectra of the other stars are shown in Table 2. The columns give, in order, the star, wavelength and identification, the type of line (*a*, *e*, P, for absorption, emission, or P Cygni), the equivalent width (W) in angstroms, the number of spectra (N) in which the line was detected, and remarks. The errors assigned to the equivalent widths reflect the formal mean error calculated from two or more exposures. The features most commonly observed are He II $\lambda 1640$ and C IV $\lambda 1550$. These lines are found in both emission and absorption, and $\lambda 1550$ is seen as a prominent P Cygni line in A78 (Heap 1979) and NGC 7094. In addition, A78 displays powerful P Cygni lines of O V and N V (again, see Heap 1979, and KF1), as does Sp-1, and He II $\lambda 2511$ is easily seen in absorption in NGC 7094. The $\lambda 2200$ interstellar absorption feature is seen in a few LWR spectra as well. Lines are listed even if they are only barely marginal identifications; see the remarks to the table. An example is O V $\lambda 1371$ in NGC 7094 (see Fig. 4), which is only suggested by a weak undulation in the continuum. These tentative detections are provided to give direction

for future observations; they should at least be checked with better exposures.

We display most of the features in Figures 4–7. In Figure 4, we show the wavelength region centered on the C IV $\lambda 1550$ line for the four stars that have (or we believe to have) strong winds: A78, NGC 7094, Sp-1, and K1-16. Figure 5 displays the $\lambda\lambda 1200$ – 1500 window for the first three of these, to show details of the N V $\lambda 1240$ and O V $\lambda 1371$ lines. In Figure 6, we look at the $\lambda\lambda 1400$ – 1700 region for nine more stars, to illustrate other lines of C IV $\lambda 1550$ and He II $\lambda 1640$. These are broken into three subsets: the first displays real or possible emission lines (A15, A20, and A65); the second, real absorption lines (A31 and Lo-1); and the third, more tenuous or only suggested features (A39, A72, Jn-1, and K1-27). Finally, Figure 7 shows the strong He II $\lambda 2511$ line of NGC 7094. The remaining He II $\lambda 1640$ lines are seen in Figures 1 and 2, so that all the lines but one of Table 2 are illustrated in some form or other. We now proceed to examine some of these features in more detail.

a) Winds in A78, NGC 7094, and Sp-1

A quick glance at Figures 4 and 5 shows that A78 and NGC 7094 have roughly comparable line widths, and consequently wind velocities, and that the Sp-1 wind is flowing considerably more slowly. A78 seems to have the highest density wind, based on the line strengths, and NGC 7094 the lowest. On the

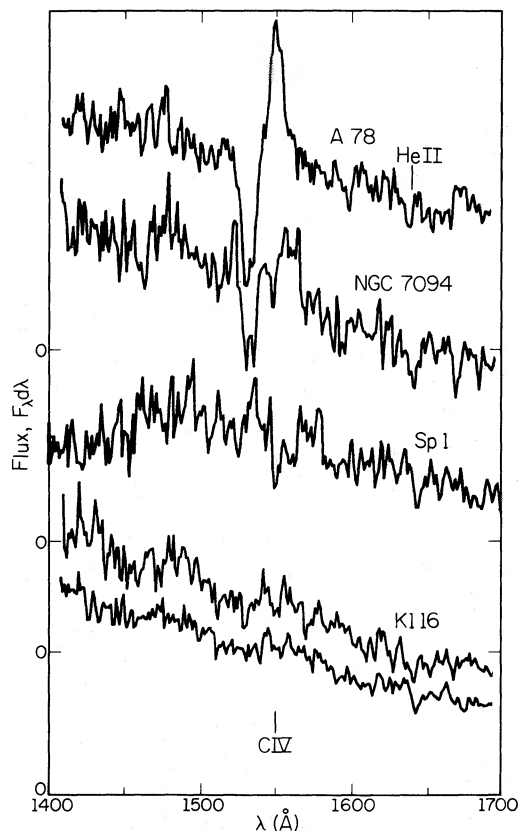


FIG. 4.—The 1400–1700 Å region for the four stars that exhibit P Cygni lines, expanded for clarity in order to show better the region of C IV and He II: A78 (SWP 16966), NGC 7094, Sp-1 (SWP 18263), and K1-16 (SWP 13550 [upper] and SWP 18640 [lower]). Sp-1 is included here because of its O v and N v features. The reality of the C IV absorption is uncertain. The case for a broad C IV P Cygni line in K1-16 is insecure, but it appears to be present in both long exposures when the break at 1460 Å is taken into account. If the line is real, the terminal velocity of the wind is about 8500 km s⁻¹. We see here that K1-16 and Sp-1, and probably NGC 7094, exhibit He II λ 1640 in absorption. Note the difference in flux for the two exposures of K1-16 (see § IVc[iv]), which are on the same scale.

other hand, Sp-1 appears to have the highest excitation, because of the strong O v and N v lines relative to uncertain C IV.

The low-dispersion mode does not lend itself well to the determination of terminal velocities unless they are high, because of the large instrumental width of the IUE. Two simplistic procedures are used here to estimate those values. First, we quadratically correct the observed terminal velocity for the instrumental width (5 Å FWHM) determined by Castella and Barbero (1983). Second, the observed terminal velocity v_{∞}^o must be an upper limit to the true value v_{∞} ; we also know from high-dispersion studies (see, e.g., Seaton 1980; Perinotto, Benvenuti, and Cerruti-Sola 1982) that the difference between the emission and absorption line centers Δv is less than v_{∞} . We can therefore determine a crude true v_{∞} by averaging v_{∞}^o and Δv .

The average of both methods gives 4500 km s⁻¹ for A78 from both C IV and O v, with a suggestion that the velocity from N v may be about 10% higher. These are essentially the results quoted by KF1. The terminal velocity for NGC 7094 derived from C IV in the same way is identical. Kaler, Mo, and Pottasch (1985) give 3900 km s⁻¹ for A78 from model fits to low-dispersion spectra, which should then apply to NGC 7094

TABLE 3
ESTIMATES OF TERMINAL VELOCITIES

Star	v_{∞} (km s ⁻¹)
A78	3900 ^a
NGC 7094	3900 ^b
Sp-1	2000: (O v) ^c 3500: (N v)
K1-16	8500

^a Adopted from Kaler, Mo, and Pottasch 1985. The simple procedure discussed in § IIa yields 4500 km s⁻¹.

^b Same line widths as A78.

^c Δv only; see § IIa.

as well. For Sp-1, the O v line has essentially instrumental width, so that only Δv is available; again, the N v velocity may be higher. These results are summarized in Table 3.

b) The Wind of K1-16

We believe also that we have evidence for a broad P Cygni profile in K1-16, but first we must examine a feature common to nearly all our spectra, a break near 1450–1470 Å. It is easily seen in the various figures, and is especially prominent in NGC 246, A51, and Ym-29, among others. The mean position of the flexure point of the break is 1457 Å. We cannot find a reasonable identification. The NBS tables for C IV (Moore 1971) show that the 5²D, 5²F, and 5²G terms have absorption heads at 1424 Å, which, given the longward confluence of bound-bound transitions, might be consistent with the obser-

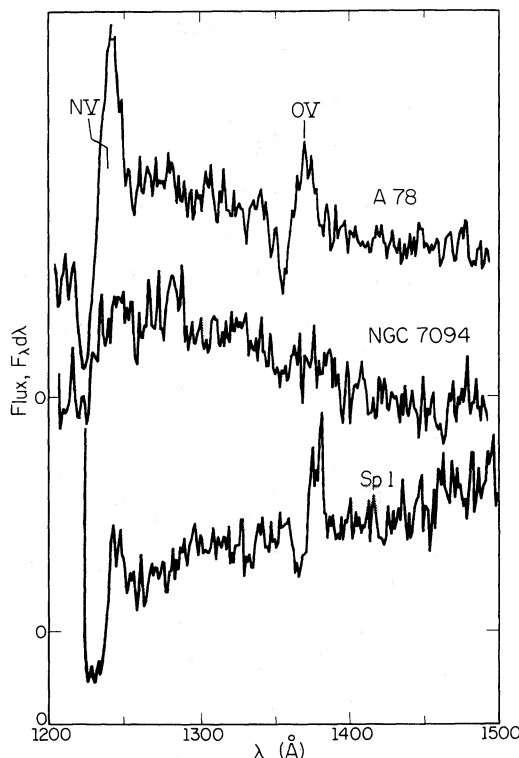


FIG. 5.—The 1200–1500 Å region for A78 (SWP 16966), NGC 7094, and Sp-1 expanded again for clarity, now to show the regions of the N v and O v lines. The lower wind velocity in Sp-1 is clearly evident. Note again the apparent feature at 1310 Å in this other exposure of A78, which KF1 tentatively identify as Si II. O v may be present in NGC 7094; the region should be examined with a longer exposure.

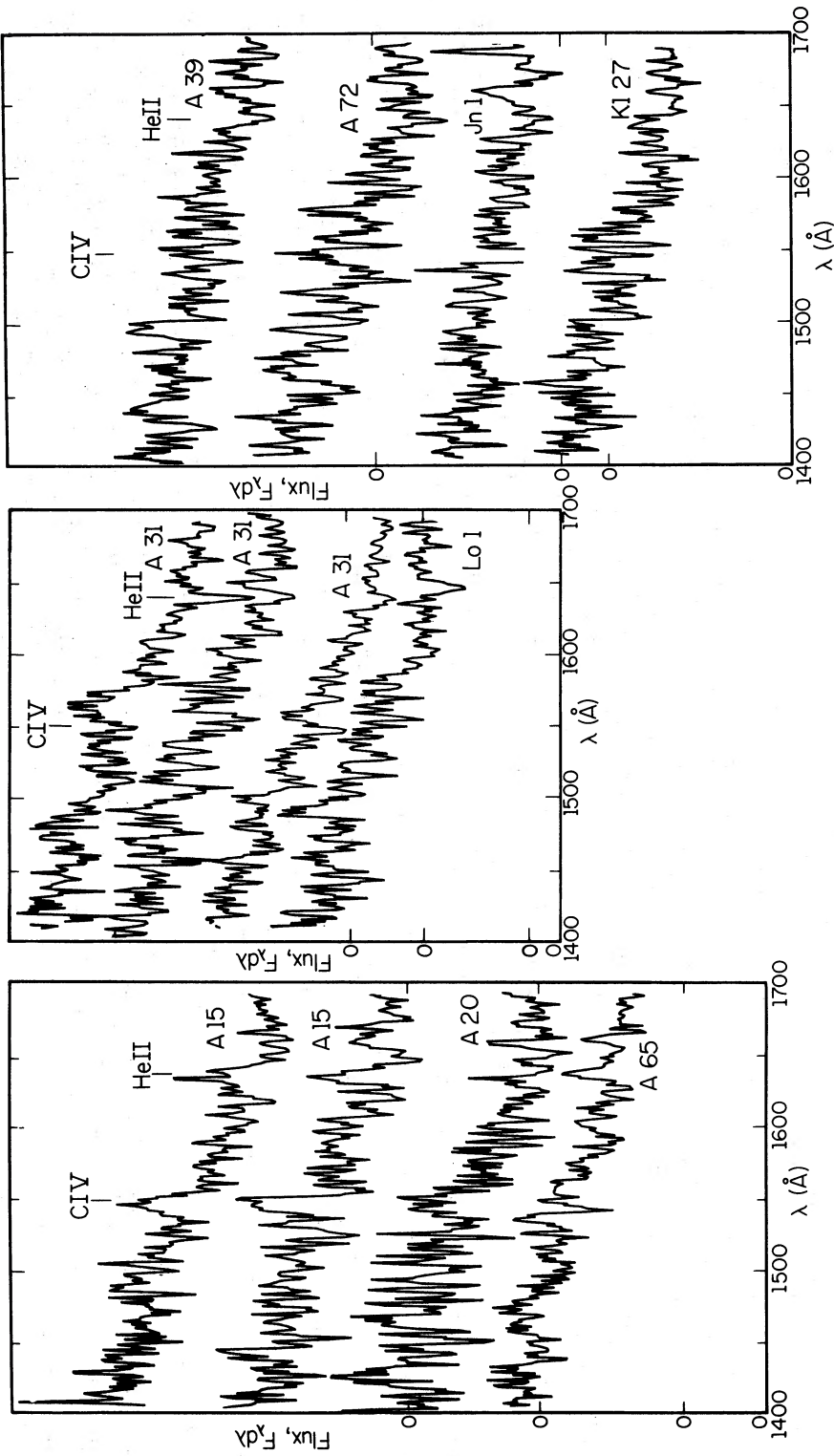


FIG. 6.—The 1400–1700 Å region for nine stars, expanded for clarity to show the C IV and He II lines. (left) A15, A20, and A65, exhibit emission, in order of decreasing probability. Both exposures of A15 (the longer on top) show C IV and He II in emission; A20 seems definitely to have C IV, though the line is nearly masked by noise; He II emission for A65 is not well established, and the star should be reobserved. (middle) A31 (SWP 13526, [top], 16970 [middle], and 18264 [bottom]) and Lo-1 clearly display He II in absorption. The bump near 1560 Å in the first exposure of A31 is spurious, as it does not appear in either of the other two. (right) A39, A72, and Jn-1 all present weaker cases for He II absorption, but it is probably there. Finally, we include K1-27, for which there is the barest suggestion of a C IV P Cygni line; this star requires further observation. The 1460 Å break is evident in several spectra.

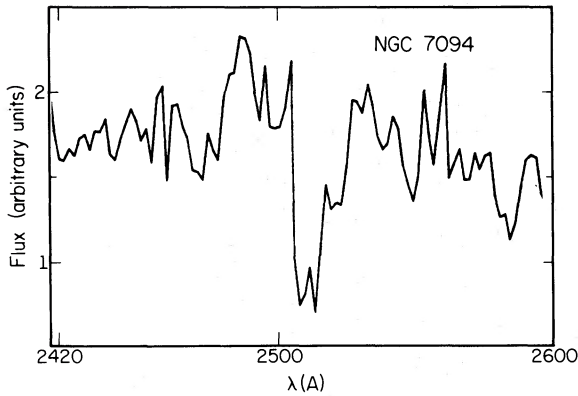


FIG. 7.—The He II $\lambda 2511$ absorption line in NGC 7094

variations. However, the C IV $\lambda 1550$ resonance line does not correlate with the strength of the feature, and in fact is usually absent. It is likely that the break, which drops the continuum by roughly 10% on the average, is due to a systematic error in the IUE data, and there is a suggestion that it is exposure-dependent: it may be more prominent on underexposed images. Also, the feature seems to be enhanced when spectra are reduced with extended-image extractions. Even though the origin of the 1460 Å break is not known, however, there is no question as to its reality.

Now return to Figure 4. K1-16 at first appears to show two broad emission features at about 1550 and 1475 Å. There is no line predicted to be at the latter of these wavelengths. If, however, we recognize the dip at 1460 Å to be the continuum break discussed above, we see that the “peak” at 1475 Å is not an emission line, but is continuum, and that the spectrum displays instead what may be absorption at about 1520 Å. The feature could be interpreted as the blueshifted P Cygni component, and the broad peak at 1550 Å as the emission component.

Is the feature real, or is it simply an artifact of exposure or reduction? In an earlier (unpublished) version of this paper, we reported on a similar broad feature seen on SWP 13526 of A31. A second, shorter exposure showed a marginal suggestion of it, but a longer one failed to exhibit any trace whatsoever; see Figure 6. Apparently, the “line” was caused by an external noise event or “hit” on the detector; a variable feature seems highly unlikely.

The case of K1-16 is different, however. The feature was found on the first exposure, SWP 13550, of 35 minutes duration. Again, a shorter, 20 minute, exposure (SWP 17235) showed a suggestion. But on a longer one, the 60 minute SWP 18640, the line emerges from the noise even more strongly. The 1400–1700 Å region is displayed for the two longer exposures in Figure 4. From their similarity, we conclude that the feature is most likely real. Some further support comes through comparison with NGC 7094, which clearly displays the C IV P Cygni line. Both appear to have He II $\lambda 1640$ in absorption (see below). Sion, Liebert, and Starrfield (1985) show the presence in K1-16 of prominent optical absorption lines of C IV $\lambda \lambda 4441$ and 4658, C III $\lambda 4650$, and He II $\lambda 4686$. An unpublished IIDS observation of NGC 7094 taken by one of us (J. B. K.) exhibits a remarkably similar spectrum, with the addition of strong Balmer lines. The presence of a P Cygni C IV profile in the ultraviolet of K1-16 is then at least consistent with the behavior of other lines.

From the two longer exposures, and with a minor correction for instrumental width, we estimate a terminal velocity of 8500 km s⁻¹, which so far as we know, is the fastest steady stellar wind known. The main source of uncertainty is the determination of the point where the apparent absorption component meets the continuum, which is in part bound up with the problem of the dip at 1460 Å.

The escape velocity can be found for K1-16 from its position on the log L –log T plane (refer ahead to Fig. 17). From the grid calculated by Kaler, Mo, and Pottasch (1985), we find that $V_{\text{esc}} \approx 1400$ km s⁻¹ for the calculated values of T and L , which, because the nebula is optically thin, are lower limits. The locus along which the star lies (see Kaler 1983a) is not far from parallel to the lines of constant v_{esc} on the plane, so that v_{esc} is not strongly dependent on optical depth, increasing at most to 2000 km s⁻¹. Thus, $v_{\infty}/v_{\text{esc}}$ ranges between 4.5 and 6, considerably higher than the nominal value of 3 found by Abbott (1978) for lower temperature stars. For A78 and NGC 7094, using Kaler, Mo, and Pottasch’s (1985) lower value of 3900 km s⁻¹, $v_{\infty}/v_{\text{esc}}$ lies between 4.3 and 4.6 and between 3.7 and 4.1 respectively (reasonably similar to that found for A78 by Heap 1982). These velocity measurements tentatively suggest an increase of $v_{\infty}/v_{\text{esc}}$ with temperature. It may be that the wind acceleration mechanism is different, or at least more efficient, at such high temperatures.

But, we must consider that these ratios are dependent on our assumptions of distance (the scale used by Cahn and Kaler 1971). In order that $v_{\text{esc}}/v_{\infty} \approx 3$ for K1-16, it would have to be at only $\frac{1}{2}$ the distance given by Kaler (1983a), which would imply a terribly tiny nebular mass of only 0.003 M_{\odot} (distance \propto mass^{0.4}). We must also consider that the P Cygni identification for K1-16 may yet be spurious, and that v_{∞} for A78 and NGC 7094 may be overestimated due to instrumental broadening and confusion. If true, however, our conclusion provides interesting clues as to the nature of the winds.

c) Other Clear Lines

In Figure 6, we show plots of the spectra of A15, A31, and Lo-1 (= K1-26) in the 1400–1700 Å window. Both scans of A15 clearly exhibit C IV $\lambda 1550$ and He II $\lambda 1640$ in emission. The latter is strong and obvious in absorption in the spectra of A31 and Lo-1. Note again the “hit” in the first plot of the latter that could be mistaken as a C IV emission line. Other unquestionably real He II $\lambda 1640$ absorptions can be seen for NGC 246 and Ym-29 in Figures 1 and 2. Finally, there is no question of the reality of He II $\lambda 2511$ in NGC 7094: see Figure 7.

d) Marginal Features

At some point, because of weakness, or underexposure, the lines slide into the noise. We know where to look, and may see a feature that may be in absorption or emission, or may simply be a fluctuation of the background. It is nevertheless worthwhile reporting on these in order to provide direction for future observations.

Lines in this category are also displayed in Figure 6. A20 and A65 seem to have emission at C IV $\lambda 1550$ and He II $\lambda 1640$ respectively; the former is fairly convincing. A39, A72, and Jn-1 appear to display He II $\lambda 1640$ absorption. This line appears probable in NGC 7094 and K1-16 (both exposures), and possible in Sp-1, all of Figure 4. K1-27 exhibits the barest suggestion of a P Cygni line at C IV $\lambda 1550$, similar to the aforementioned O V $\lambda 1371$ line in NGC 7094 (see Fig. 5).

TABLE 4
OBSERVED CENTRAL STAR FLUXES

STAR	$10^{13} F(\lambda)d\lambda$ (ergs cm ⁻² s ⁻¹ Å ⁻¹)								NOTES
	$\lambda = 1300$ Å ^a	1500 Å	1750 Å	1850 Å	2070 Å	2270 Å	2350 Å	2950 Å	
NGC 246	163s	88.9	46.1	39.5	22.7	15.5	14.0	6.5	
	138	80.0	43.9	37.1	22.4	15.4	13.2	7.1	
NGC 2438	0.278	1
NGC 2474-2475	1.10s	0.70	0.32	0.29	
NGC 2610	2.29	1.47	0.88	0.72	0.39	0.27	0.28	0.14	2
NGC 6058	19.9s	12.0	6.55	5.40	3.52	2.27	2.25	1.07	
NGC 7008	0.30	3
NGC 7094	13.7	9.49	5.60	4.63	2.33	1.70	1.57	1.08	
IC 5148-50	2.94S	1.67	0.84	0.70	
	2.85	1.62	0.84	0.70	
	2.82	1.64	0.82	0.73:	
A15	267s	1.63	0.84	0.69	
	2.12	1.41	0.81	0.69	
A20	1.09	0.76	0.42	0.33	
A28	0.43	0.23	0.17	0.12	4
	0.81	0.51	0.29	0.24	5
A31	4.39	2.44	1.39	1.07	
	3.88	2.50	1.37	1.14	0.51:	0.39:	0.36:	0.18:	
	4.18S	2.52	1.35	1.08	
A33	3.17s	1.78	0.92	0.75	
	2.79	1.67	0.86	0.75	0.55:	0.26:	0.21:	0.13:	
A34	1.97s	1.07	0.63	0.47	
A36	145	87.5	48.3	39.8	22.0	14.4	13.5	7.54	
A39	2.44	1.77	1.06	0.90	
A43	2.11	1.55	1.06	0.80	5
A51	1.15	0.99	0.55	0.45	
A65	1.03	0.65	0.37	0.30	
A72	1.54	1.06	0.64	0.53	
A78	19.6s	12.2	7.36	5.97	3.22	2.32	2.24	1.50	
	16.9	11.0	7.22	6.11	3.75	2.38	2.31	1.46	
	17.0	10.8	6.88	5.75	3.25	2.44	2.22	1.53	
A82	0.069	0.208	0.160	0.150	6
Jn-1	0.60	0.43	0.25	0.20	7
K1-14	0.98	0.76	0.51	0.38	5
K1-16	8.90	4.76	2.87	2.18	8
	8.33s	4.79	2.34	2.06	0.87	0.85	0.81	0.79	
	7.06	4.25	2.18	1.98	
	6.43S	3.61	1.88	1.53	
	7.50	4.42	2.67	2.17	
	7.50	4.58	2.58	2.25	
	7.58	4.42	2.33	1.92	
	7.42	4.67	2.33	1.83	
K1-22	0.34:	0.31:	0.10:	0.10:	5
K1-27	1.85	1.12	0.63	0.50	
K3-27	0.31	0.28	0.14	0.13	5, 9
Lo-1	6.08	3.84	2.01	1.68	
LoTr-5	13.2s	7.67	3.67	3.17	
	13.2	7.17	4.00	3.25	
	13.5	7.33	3.67	3.08	
	11.5	7.00	3.83	3.07	
Sp-1	0.28	0.51	0.30	0.24	5
	0.50	0.68	0.40	0.28	
Ym-29	2.00	1.33	0.78	0.67	

^a The letters s and S indicate mild and severe saturation; fluxes determined from IUE extrapolation procedures.

NOTES.—(1) Confusion at wavelengths ≥ 1500 Å with either optical companion or nebular continuum. (2) Possible contamination by nebular continuum. (3) Reddening so high that only longest wavelength could be observed. (4) Star set at edge of aperture; absolute fluxes too low. (5) Considerably underexposed—high error (see § III). (6) Probably not the true central star, see § IVc(iii); fluxes presented for the longer exposure only. (7) Fluxes may be low due to aperture effect, see text. (8) Exposures made in a single shift are enclosed in braces. (9) Probably contaminated by nebular continuum, which may be $\sim 10\%$ of the total.

Finally, He II $\lambda 2734$ is suggested on one exposure of A78 (not illustrated); however, He II $\lambda 1640$ and He II $\lambda 2511$ are *not* detected.

e) The 2200 Å Interstellar Bump

Some of our stars exhibit the broad absorption imposed at 2200 Å by interstellar dust (see, for example, Savage and Mathis 1979, hereafter SM). We readily detect it in the LWR spectra of A78 and NGC 7094 and discuss both cases in KF1, where we provide an illustration for the former. The feature is also to be seen in the spectrum of NGC 6058 in Figure 1. In addition we can detect it in NGC 2610 and A36, and possibly in NGC 246. The stars for which the absorption is seen are listed in Table 2, along with the intrinsic stellar features. We will discuss the quantitative measurement of the 2200 Å bump below in the section on photometry.

III. ULTRAVIOLET PHOTOMETRY

a) Observed Fluxes

We present our initial photometric results in Table 4, where we sample the UV spectra at eight wavelengths: 1300, 1500, 1750, 1850, 2070, 2270, 2350, and 2950 Å. Full spectral details will be given in later papers, as they were for A78 in KF1. We chose the first three LWR points ($\lambda > 2000$ Å) on the basis of the SWP wavelengths in order to span the 2200 Å bump, such that we have flux pairs with zero extinction differences: 1300, 2070, and 2270 Å all have the same extinctions on the basis of the SM curve, as do 1500 and 2350 Å. The 2950 Å point is added for its proximity to the ground-based UV for an eventual tie-in with optical observations.

We give all fluxes at these eight points in units of 10^{-13} ergs $\text{cm}^{-2} \text{s}^{-1} \text{Å}^{-1}$ for all exposures. We indicate mild saturation by lower case *s* next to the value, and severe saturation by capital *S*.

b) Errors

We evaluate random errors by comparing fluxes from the multiple exposures taken of several stars. We exclude three: (1) A28, since for the first exposure the star was set at the edge of the aperture, and the fluxes are clearly too low; (2) K1-16, since there is evidence for intrinsic variability (see § IVc[iv]); and (3) Sp-1, because the first observation was seriously underexposed. That leaves seven stars with more than one observation, for which the exposures ranged from adequate to good.

In order to derive a typical error for an individual flux measurement, we first derive a mean at each wavelength for each object, weighted proportionally to exposure time, where we exclude saturations. We then compute the formal mean error for a single data point. These values range from near zero (which one occasionally expects out of simple coincidence, given the low number of data points) to an extreme high of about $\pm 10\%$. Since we are dealing with low-number statistics, we assume that the error to be assigned to a single point is the mean of all the 25 mean errors, which is $\pm 3.9\%$.

We derive the same figure if we use only those four stars with three or more exposures (IC 5148-50, A31, A78, and LoTr-5). If we apply this technique to the two stars with multiple LWR exposures (NGC 246 and A78), we again derive $\pm 3.9\%$.

We thus assume that the internal random error to be applied to the fluxes with adequate exposures is $\pm 4\%$. Six observations are notably underexposed, however: the second of A28, the first of Sp-1, and those of A43, K1-14, K1-22, and K3-27.

Two observations were made of Sp-1, and from comparison of the flux pairs, we find a mean error of $\pm 18\%$. Since the first exposure of this star is quite poor, we simply average this figure with the previous value to obtain an error of $\pm 10\%$ to be applied to A28, A43, K1-14, and K3-27, and adopt $\pm 15\%$ for K1-22. Errors in flux ratios, and systematic errors, which include changes in the sensitivity of the detectors, will be discussed later, in §§ IVd(ii)–IVd(iv).

IV. ANALYSIS OF THE PHOTOMETRY

In this section, we establish properties of the stars, derived in part from the ultraviolet data presented in Table 4. We show the first part of the results of these investigations in Table 5. Before we proceed to a discussion of the table, we first give, in column (2), the visual magnitudes that we adopt for each star that are needed for a quantitative visual reference base.

We give the reference for each magnitude in column (3) and supply the key in note a. We select preferentially in the order AB, SL, photographic (AB, KO, KF, AN), and estimate (VV, KO1). The errors assigned are discussed by Kaler (1983a). Although the SL magnitudes are subject to systematic error due to inclusion of nebular continuum (Shaw and Kaler 1985), the nebulae discussed here have such low surface brightnesses that the magnitudes should generally be quite accurate. The corrections to the photographic magnitudes suggested by Shaw and Kaler (1985) are not applied, since the stars are generally much fainter than those included in their calibration.

a) Interstellar Extinction

The ultraviolet data are very sensitive to interstellar reddening and must be corrected with care. Unfortunately, nebular data, specifically Balmer decrement intensities, are not yet available with sufficient accuracy for most of the objects considered here. Consequently, for most of our survey, we rely on the color excesses as determined from the *B* and *V* magnitudes of the nuclei. This procedure does have the advantage of allowing for possible circumstellar dust that would not be detected via nebular photometry, as in the case for A30 (Greenstein 1981). However, it presents two problems: the establishment of the unreddened $(B-V)_0$, and the relation of color excess to total extinction. We simplify the procedure by adopting common, typical values for all our stars.

Allen (1973) gives $(B-V)_0 = -0.46$ for an infinitely hot blackbody, which by comparison with nebular extinctions for nearby planetaries is clearly too low; see Kaler (1983a), Table 3. Cahn (1984) gives $(B-V)_0 = -0.38$ (the value used by Kaler 1983a) for infinite temperature, but for temperatures typical of the stars discussed here (130,000 K; see below), his formula yields $(B-V)_0 = -0.34$. This value is too high, since several well-observed stars have smaller observed colors. We use two approaches. First, we adopt the Wesemael *et al.* (1980) line-blanketed hydrogen models for $\log g = 6.0$ and extrapolate their calculated color to 130,000 K to find $(B-V)_0 = -0.375$, which we round to -0.38 .

Next we plot the distribution of colors from Abell (1966), and those of low surface brightness nebulae from Shao and Liller (1973); see the discussion above. The distribution is continuous down to $B-V = -0.37$, at which point it stops abruptly; two stars are well below this value, Jn-1 at -0.41 and NGC 3587 at -0.45 . Given these two, and that we might still expect some small residual extinction at the end of the continuous distribution, we believe that $(B-V)_0 = -0.38$ is

TABLE 5
EXTINCTIONS AND MAGNITUDES

Star (1)	Observed V (2)	Reference ^a (3)	c (4)	Reference ^b (5)	Mean Observed $10^{13}F(\lambda 1500)$ (6)	$V(UV)$ (7)	$V(UV, T_c)$ (8)	Notes
NGC 246	11.95 ± 0.01	SL	0.01 ± 0.02	$B-V$	85.9 ± 4.0	11.84	...	
NGC 2438	17.5	AN	0.20 ± 0.03	TPP	...	17.84	17.88	1
NGC 2474-2475	17.2 ± 0.4	KO	0.0 ± 0.05	K83	0.70	17.09	17.43	
NGC 2610	15.5 ± 0.1	SL	0.12 ± 0.03	TPP	1.47	15.88	15.77	2
NGC 6058	13.70 ± 0.01	SL	0.10 ± 0.02	$B-V$	12.0	13.67	...	
NGC 7008	13.26 ± 0.05	SL	1.18 ± 0.10	$B-V$...	13.29	...	3
NGC 7094	13.61 ± 0.01	SL	0.18 ± 0.02	$B-V$	9.49	13.65	...	
IC 5148-50	0.0 ± 0.11	b	1.65 ± 0.02	16.16	16.51	
A15	15.72 ± 0.01	AB	0.10 ± 0.02	$B-V$	1.57 ± 0.10	15.88	...	
A20	16.56 ± 0.01	AB	0.16 ± 0.02	$B-V$	0.76	16.47	...	
A28	16.4 ± 0.3	AB, KO	0.0	K83	0.51	17.44	17.37	4, 5
A31	15.51 ± 0.01	AB	0.10 ± 0.02	$B-V$	2.49 ± 0.03	15.38	...	
A33	15.54 ± 0.01	AB	0.31 ± 0.02	$B-V$	1.74 ± 0.05	15.07	...	
			0.0 ± 0.28	K83	...	16.11	...	
A34	16.32 ± 0.01	AB	0.17 ± 0.02	$B-V$	1.07	16.06	...	
A36	11.51 ± 0.01	AB	0.07 ± 0.02	$B-V$	87.5	11.62	...	
A39	15.76 ± 0.01	AB	0.07 ± 0.02	$B-V$	1.77	15.85	...	
A43	14.71 ± 0.01	AB	0.28 ± 0.02	$B-V$	1.55	15.29	...	5
A51	15.42 ± 0.01	AB	0.37 ± 0.02	$B-V$	0.99	15.47	...	
A65	15.90 ± 0.01	AB	0.66 ± 0.02	$B-V$	0.65	14.95	15.30	
			0.19 ± 0.24	K83	...	16.54	...	
A72	16.12 ± 0.01	AB	0.07 ± 0.02	$B-V$	1.06	16.41	...	
A78	13.25 ± 0.01	AB	0.18 ± 0.02	$B-V$	11.6 ± 0.5	13.44	...	6
A82	13:	VV	0.75 ± 0.25	IIDS	0.208	> 16.7	...	7
Jn-1	16.13 ± 0.01	SL	0.00 ± 0.02	$B-V$	0.43	17.63	17.40	8
K1-14	16.1 ± 0.5	KF	0.00 ± 0.05	IRS	0.76	17.01	16.37	5
K1-16	15.09 ± 0.01	SL	0.04 ± 0.02	$B-V$	4.44 ± 0.14	14.95	...	9
K1-22	17.5 ± 0.5	KF	0.29 ± 0.34	K83	0.31:	17.00	17.35	5
K1-27	16.0:	KO1	0.00 ± 0.10	b	1.12	16.57	16.72	
K3-27	18.3:	K81	0.28 ± 0.03	IRS	0.28	17.14	17.16	5, 10
Lo-1	14.0:	KO1	0.00 ± 0.05	b	3.84	15.23	15.35	
LoTr-5	0.00 ± 0.10	b	7.41 ± 0.14	14.53	14.88	
Sp-1	13.87 ± 0.01	SL	1.16 ± 0.02	$B-V$	0.64 ± 0.08	13.46	...	11
Ym-29	15.99 ± 0.01	AB	0.08 ± 0.02	$B-V$	1.33	16.13	...	

^a AB, Abell 1966. AN, Anderson 1934; V is set equal to his photographic value. K81, Kaler 1981. KF, This paper; photographic magnitude determined from stellar diameter on POSS by calibration of King and Raff 1977, converted to V via extinction and an assumed intrinsic color of -0.38 . KO, Kohoutek, in Perek and Kohoutek 1967. KO1, Kohoutek 1977; blue magnitude estimate converted to V as in KF above. SL, Shao and Liller 1973, quoted by Acker *et al.* 1982. VV, Vorontsov-Velyaminov 1961.

^b b , estimated to be zero because of high galactic latitude. $B-V$, from stellar color and $(B-V)_0 = -0.38$. IIDS, IRS, unpublished Kitt Peak observations of the $H\alpha/H\beta$ ratio with the instrument named K83, Kaler 1983a. TPP, Torres-Peimbert and Peimbert 1978.

NOTES.—(1) Longer wavelengths contaminated (see § I); $V(UV)$ calculated from $F(\lambda 1300)$; T_c is assumed to be T_2 . (2) Possible contamination by nebular continuum. (3) Only longer LWR wavelength region observed because of high extinction: $V(UV)$ calculated from $F(\lambda 2950)$. Iteration on λ_{eff} of B filter (§ IVa) yields $c = 1.31$ and $V(UV) = 13.73$. $B-V$ or $F(\lambda 2950)$ is probably in error. (4) First exposure, star at edge of aperture; second exposure used for fluxes, and that is suspect because of high $V(UV)$. (5) Error in flux assumed to be $\pm 10\%$ because of underexposed image; $\pm 15\%$ for K1-22. (6) Extinction from optical energy distribution derived by KF1. (7) Not true central star, see text; lower limit calculated from $F(\lambda 1300)$; only second exposure used. (8) Star may be at edge of aperture. (9) $F(\lambda 1500)$ is a straight mean of all exposures because of possible stellar variability. (10) Magnitude may be increased by about 0.1 to allow for nebular continuum. (11) Iteration (see note 2) yields $c = 1.29$ and $V(UV) = 13.87$.

quite reasonable on empirical grounds as well, so we adopt this value as standard.

In order to express reddening, we use the logarithmic extinction at $H\beta$, c , ordinarily employed in nebular studies. From B and V effective wavelengths, and the standard Whitford (1958) curve, we can express c in terms of color excess as $c = KE_{B-V}$, where K is a ratio of total-to-selective extinction, obviously related to the usual R . The constant of proportionality will vary as a function of temperature (T) and reddening because of changes in effective wavelength, particularly for that of the B filter. From the data in Allen (1973), we find that for a blackbody at 130,000 K, K increases from 1.38 at $c = 0$ to 1.65 at $c = 1.50$. Thus the calculation of extinction from stellar colors is iterative, but with rapid convergence. Since most of our extinctions are low, by reason of observational selection, we simply choose a typical value of $c = 0.15$, for which $K = 1.41$.

Some error in c will arise from the use of constant values (T and K), but it will be small and lost within other errors and uncertainties. Extinctions calculated in this way will be somewhat underestimated for values significantly greater than 0.1. Where the magnitudes are not accurately known, we use both published and unpublished nebular $H\alpha/H\beta$ ratios to calculate c or assume the extinction to be zero on the basis of high Galactic latitude.

The adopted extinction constants are presented in column (4) of Table 5, with references or a code to the method in column (5). Errors are calculated from those assigned to B and V , from the errors assumed to apply to the nebular data or from the likely error for a given Galactic latitude.

For most of our stars, $c(B-V)$ is consistent with those values determined by other methods. But in the case of NGC 7008, the $B-V$ extinction of 1.17 (1.31 with the proper

iteration), which produces consistent predicted and observed V magnitudes (§ IVc), is considerably higher than the value of 0.84 ± 0.14 found from the $H\alpha/H\beta$ ratio by Kaler (1983b), the radio extinction of 0.66 ± 0.14 given by Cahn (1974), or the extinction derived from the published Balmer decrements (see also Cahn 1974). Circumstellar dust may be involved, as Greenstein (1981) showed for A30, or the color may be in error. A similar anomaly is found for A51, for which the extinction in Table 2 ($c = 0.35$) is significantly larger than the one found from $H\alpha/H\beta$ (0.0 ± 0.19) by Kaler (1983a). Alternative values are given in Table 5 for both A33 and A65.

b) Extinctions from the 2200 Å Bump

Since some of our spectra exhibit the 2200 Å interstellar feature (§ IIe), we have an additional opportunity to determine an extinction constant. A common procedure is to correct the LWR spectrum with a variety of color excess values until the bump visually, and subjectively, disappears. This procedure will surely carry a significant error, and it is nearly useless for low extinctions where the bump is only barely evident.

Clearly, quantitative methods can and should be used instead. We employ here the same procedures that we used to evaluate the extinction for A78 and NGC 7094 in KF1, where we again use the SM reddening function. There, we sampled the UV spectra every 10 Å over different wavelength intervals around 2200 Å. We dereddened the data by incrementing c in steps of 0.01 and fitted the results to a blackbody appropriate to the ultraviolet color temperature (§ IVd[ii]) until we found the value at which the sum of the squares of the percentage deviations was a minimum. We calibrated the method on nebular observations of NGC 7094 and found that we achieved consistent results if we averaged the 2200 Å extinctions determined from fits over three separate wavelength intervals, $\lambda\lambda 1800\text{--}2400$, $\lambda\lambda 2000\text{--}2400$, and $\lambda\lambda 2200\text{--}2400$. We present the results of the analysis in Table 6, where we list in columns (2)–(5) the individual extinctions from the above three wavelength intervals and the mean \bar{c} . The error is the mean error found from the three values coupled with the uncertainty in the fit to NGC 7094 (see KF1).

In column (6) we give alternative extinction values, primarily those from Table 5 but embellished with some others. For four stars, \bar{c} agrees well with $c(\text{other})$, but for two, A36 and espe-

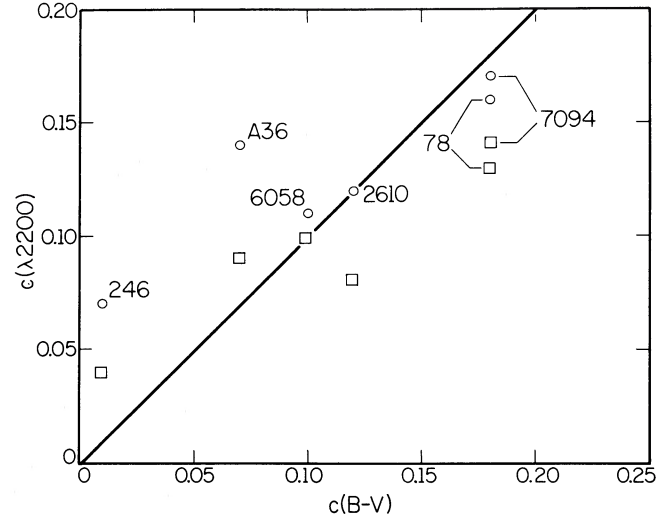


FIG. 8.—The extinctions derived from the 2200 Å feature plotted against $c(B-V)$ for all the stars of Table 6 except A78, where the extinction derived from the optical flux derived by KF1 is used. Circles, $\bar{c}(\lambda 2200)$, the average of three separate fits between $\lambda\lambda 1800\text{--}2400$, $\lambda\lambda 2000\text{--}2400$, and $\lambda\lambda 2200\text{--}2400$; squares, $c(\lambda\lambda 2000\text{--}2400)$ alone.

cially NGC 246, the former is uncomfortably large. The fit for these is better if we use only the $\lambda\lambda 2000\text{--}2400$ value from column (3). The extinctions from $\lambda\lambda 2000\text{--}2400$ and the \bar{c} are plotted in Figure 8 against the $c(\text{other})$ that we use in Table 5. We see that both sets of points correlate but that the slope is less than 45° . At low extinction, $c \leq 0.10$, we should use $c(\lambda\lambda 2000\text{--}2400)$, but above that value \bar{c} is better. The small anomaly may reflect systematic errors in the fluxes. The correlation should be extended with similar calculations to higher extinctions.

c) UV Fluxes and Visual Magnitudes

We can use a flux observed in the UV to calculate a visual magnitude, which we call $V(\text{UV})$. In the case of photoelectrically measured magnitudes (those with errors ≤ 0.01 in Table 5), this procedure provides a good internal check on apparent UV and visual luminosities and on the interstellar extinction constants. For the remaining stars, such a computa-

TABLE 6
EXTINCTION CONSTANTS FROM 2200 Å

STAR (1)	c (individual)			\bar{c} (5)	c (other) (6)	Reference (other) ^a (7)
	$\lambda\lambda 1800$ –2400 (2)	$\lambda\lambda 2000$ –2400 (3)	$\lambda\lambda 2200$ –2400 (4)			
NGC 246	0.08	0.04	0.08	0.07 ± 0.02	0.00 ± 0.03	IRS (unpublished)
	0.01 ± 0.02	$B-V$ (SL)
NGC 2610	0.15	0.08	0.13	0.12 ± 0.04	0.12 ± 0.03	TPP
NGC 6058	0.18	0.10	0.06	0.11 ± 0.04	0.10 ± 0.02	$B-V$ (SL)
	0.04	K85
NGC 7094	0.13	0.14	0.24	0.17 ± 0.06	0.17 ± 0.04	KF1
	0.18 ± 0.02	$B-V$ (SL)
A36	0.14	0.09	0.18	0.14 ± 0.05	0.07 ± 0.02	$B-V$ (SL)
A78	0.19	0.13	0.17	0.16 ± 0.05	0.24 ± 0.02	$B-V$ (AB)
	0.27 ± 0.02	$B-V$ (SL)
	0.18 ± 0.01	$F(\lambda)(\text{KF1})^b$

^a K85, Kaler 1985b; all other references as in Table 5.

^b Preferred value; see KF1 for details.

tion provides the best way to improve or establish visual magnitudes; note that three have no measured, or even estimated, values at all.

We use 1500 Å as our basic UV wavelength. We present the mean 1500 Å fluxes in column (6) of Table 5, where we average multiple exposures by weighting proportionally to exposure time, except for K1-16, for which we give a straight mean (see § IVc[iv]). The errors are the mean errors of the mean. Those to be applied to single exposures can be taken as $\pm 4\%$ ($\pm 10\%$ to $\pm 15\%$ for the stars with poorer data; see § IIIb).

We first calculate the $V(\text{UV})$ magnitudes by assuming: (1) the extinction constants in column (4); (2) the SM extinction curve coupled to the Whitford function, scaled such that $f(\lambda)$, the combined function, is -1 at $\lambda = \infty$ and 0 at $H\beta$, as per standard nebular practice [$\Delta f = f(\lambda 1500) - f(\lambda 5480) = 1.35$]; (3) a blackbody at 130,000 K [for which $F(\lambda 1500)/F(\lambda 5480) = 132$]; and (4) an effective V wavelength of 5480 Å (corrections to the effective wavelength of the V filter for the temperatures adopted here are of little consequence, so we shall continue to refer to 5480 Å); (5) the calibration of Oke and Schild (1970) of visual magnitude in terms of flux at 5480 Å (also adopted by Oke and Gunn 1983, who take only a slightly different value, 0.005 mag, for the magnitude of Vega.) The above characteristic temperature is the one that gives the best fit between the observed photoelectric and the calculated values (i.e., $\langle V(\text{obs}) - V(\text{UV}) \rangle = 0$), excluding Jn-1 and A65, which are both clearly anomalous, and NGC 2610 for which the $V(\text{obs})$ error is ± 0.1 .

There are two exceptions to the standard procedure. NGC 7008 is highly reddened, and we have fluxes from the LWR only longward of 2850 Å; we choose 2950 Å as our reference wavelength. NGC 2438 appears to be contaminated with nebular continuum at longer wavelengths, and we are able to determine a clear stellar flux only at the shortest wavelength of 1300 Å. See Table 4 for the fluxes.

We place the results of our calculations in column (7) of Table 5. We plot $V(\text{UV})$ against $V(\text{obs})$ in Figure 9, where the 18 stars used in the temperature calibration are given as open circles. Note the close adherence to the 45° slope. The errors can be assessed by examining $V(\text{obs}) - V(\text{UV})$; we find that two-thirds of the differences fall within ± 0.17 mag, which we adopt as the error to be applied to $V(\text{UV})$, including those for which no photoelectric values are available.

We can improve the magnitudes if we know the proper color temperature T_c that connects the UV with the optical. In the next section we derive these from various flux ratios. We anticipate these results (which are given in col. [8] of Table 7), and recalculate what we now call $V(\text{UV}, T_c)$, wherein we substitute $F(\lambda 1500)/F(\lambda 5480)$ calculated from a blackbody at temperature T_c for the coefficient 132 in assumption (3) above. These magnitudes are given in column (8) of Table 5 for the stars without accurate photoelectric determinations or for those with some associated anomaly. There is no point in calculating $V(\text{UV}, T_c)$ for the others, since the flux ratio $F(\lambda 1500)/F(\lambda 5480)$ is used for them in the calculation of T_c .

The stars for which we derive $V(\text{UV}, T_c)$ are also plotted in Figure 9, where open and closed symbols represent $V(\text{UV})$ and $V(\text{UV}, T_c)$ respectively. The stars fall into three categories, which we discuss in the following subsections.

i) Anomalous Magnitudes

We find anomalies for three stars, A65, Jn-1, and A28. In the case of A65, the two available values of c are quite different,

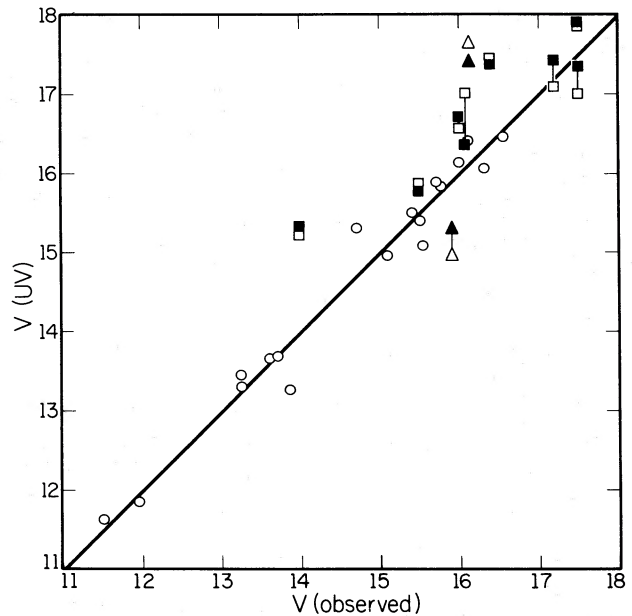


FIG. 9.—The V magnitudes predicted from the fluxes at 1500 Å, the observed interstellar extinctions, and an assumption that the stars behave like blackbodies at a specific temperature T , plotted against the directly observed values. Circles, photoelectric V magnitudes; squares, photographic V magnitudes; triangles, anomalous data (A65 and Jn-1); open symbols, calculations for $T = 130,000$ K, which provide the best fit to the photoelectric magnitudes; filled symbols, $T = \langle T_c \rangle$ for a blackbody, from Table 7. If two points for the same star are separated, they are connected by a line. K3-27 is excluded from the figure. The heavy solid line is the 45° slope.

and the $V(\text{UV})$ derived from each of them bracket $V(\text{obs})$; agreement is attained if $c = 0.35$. The extinction should be derived from additional observations of nebular $H\alpha$ and $H\beta$.

For Jn-1, there is little doubt about the extinction: Kaler (1983a) gives $c = 0$ from nebular $H\alpha/H\beta$ (supported by unpublished Kitt Peak intensified Reticon scanner data), which agrees with the stellar color. Kohoutek's photographic blue magnitude (see PK) agrees well with SL, as does a remeasurement from the POSS with the scale of King and Raff (1977). The *IUE* photowrite shows that the image is very close to the edge of the aperture as indicated by geocoronal Lyman- α , and the $F(\lambda 1500)$ flux may be low because of lost light. However, Ym-29 and two of the three exposures of A31 are similarly placed, and for these, $V(\text{obs})$ and $V(\text{UV})$ agree well.

The magnitude of A28 was estimated photographically from the POSS. However, Abell's and Kohoutek's determinations agree, and these are also supported by our remeasurement. The first exposure, which we do not use here, was taken clearly on the edge of the aperture. The second is well-centered in the aperture in one dimension, but from the earlier blind offset difficulty that we experienced, we suspect that we may have lost light in the second exposure as well. All three stars should be remeasured optically, and Jn-1 and A28 with the *IUE* with more precisely known offsets.

ii) Improvements in Earlier Magnitudes

Three stars in the list (aside from A28) have photographically determined magnitudes that can be improved by the ultraviolet observations. As for A28, V for NGC 2474-2475 was found from the POSS; $V(\text{UV})$ and $V(\text{UV}, T_c)$ are in excellent agreement with it, and the latter is probably a slight betterment. The magnitudes of Lo-1 (K1-26) and K1-27 were

merely estimated by Kohoutek (1977) from the Southern Sky Survey. The $V(UV, T_c)$ values are a clear improvement. SL give V only to the nearest tenth for NGC 2610, with a note that it might be variable. Assuming constancy, our value is probably more precise.

SL also found V equal to 15.09 for NGC 2438. Curtis's (1918) photo (see Fig. 10 [Pl. 14]) shows that the true nucleus has a bright optical companion, which was most likely the one measured by SL. Anderson (1934) found a photographic magnitude of 17.5 for the correct star, which, given his accuracy, is adopted for V as well. Our determination shows it to be only somewhat fainter. Because the spectrum is contaminated at longer wavelengths (see § I), we calculated our V from the flux at 1300 Å. K3-27, for which SL found $V = 13.84$, presents a different problem in contamination. Kaler (1981) found a blue magnitude of roughly 18.1, which from the extinction yields $V \approx 18.3$, and which implies that SL measured only nebular continuum. Our new value is consistent with this result.

Finally, we update our earlier magnitude from Feibelman and Kaler (1983) for the nucleus of LoTr-5, the companion to the G giant SAO 82570, and determine for the first time a V magnitude for IC 5148–5150.

iii) *New Identifications*

This section strongly overlaps with the one above, in that we are determining new magnitudes, but this time for the correctly identified star. The problem is similar to that for NGC 2438 described above: the K1-14 and K1-22 nuclei both have brighter close companions that were at first assumed to be the central stars; see Figure 10.

SL give $V = 13.25$ for the central star of K1-14. The smaller photo of K1-14 in Figure 10, enlarged from the POSS, shows two stars within the nebula. The stellar image sizes and the King and Raff (1977) calibration yields $V = 13.4$ for the brighter of the two and 16.1 for the fainter (Kaler 1981), assuming that both are hot and $c = 0$. The $V(UV, T_c)$ then seems to indicate that the latter is the true nucleus. But the larger, higher resolution photograph, kindly made available to us by Dr. Franco Sabbadin, illustrates the severe difficulty that can beset these identifications. The more detailed image shows yet a third star about 2" southwest of the bright one at the center and blended with it. Since it is most nearly centered and has about the same magnitude as the star first suspected, it undoubtedly is the true nucleus.

In his discovery photo of K1-22, Kohoutek (1971) points out three stars near the center (see Fig. 10), and suggests the brighter one as the nucleus, for which he gives a photored magnitude of 16.6 (only the red Whiteoak field is available). Comparison of his red and blue magnitudes in PK for hot stars of zero extinction, together with $B - V = -0.4$, yields $V = m_{\text{red}} - 1.2$. With $c = 0.38$ for K1-22, we assume $V - m_{\text{red}} = -1.0$ and find $V = 15.6$. With the King and Raff scale and the same correction, we find $V = 14.9$. The *IUE* aperture excluded the fainter star 15" west of the brighter one but should have encompassed the faintest of the three 4" east, which we estimate from the above procedure as having V between 17.0 and 17.5. The $V(UV)$ for $c = 0$ and $c = 0.29$ bracket this range, strongly suggesting that the faint easternmost of the trio is the true nucleus. However, Smith and Gull (1975) present an objective prism spectrogram that shows the brightest of the three to be very blue, indicating that Kohoutek's candidate may indeed be the correct central star. These stars must both be examined optically to resolve the conflict.

Finally, A82 poses a dilemma. Kaler (1983a) pointed out that the star suggested as the nucleus and estimated as 13th mag by Vorontsov-Velyaminov (1961), could not be correct. Kaler and Shaw (unpublished) observed the system with the IIDS and found this bright, centrally located star to be of class K with a B magnitude of 16.2 and derived an extinction of 0.75 ± 0.25 to the nebula from the $H\alpha/H\beta$ ratio. We observed this star with the *IUE*, thinking that we might uncover a binary as we did for LoTr-5 (Feibelman and Kaler 1983). In both exposures we did indeed detect ultraviolet radiation, but the interpretation is ambiguous. If we deredden the fluxes with the nebular extinction, the energy distribution is consistent with a B star at $\sim 25,000$ K (see § IVd), much too cool. If we assume that the nucleus is surrounded by circumstellar dust and derive the extinction from the $\lambda 1300/\lambda 1750$ ratio for a 10^5 K blackbody, $c = 1.32$; the dereddened $\lambda 1500/\lambda 1850$ ratio would be consistent with 10^5 K, but the $\lambda 1500$ flux would predict $V = 13.8$, much too bright. The UV radiation may be coming from an early-type field star within the aperture, but it is hard to find a combination of reddening and temperature that would render it sufficiently faint on the POSS. If we assume that $T = 10^5$ K, the maximum extinction and use our flux of 0.07 at 1300 Å, we derive a magnitude limit of $V \geq 16.7$. The POSS prints show a star slightly off center with a blue magnitude of 18.7 4" northwest of the K star which is a candidate, although a very unlikely one. The next steps in the identification of the true nucleus would be to take an optical spectrogram of this fainter star and high-resolution images of the field inside the nebula. We may well have a situation similar to that discussed above for K1-14.

iv) *The Variable Nature of K1-16*

Not only does K1-16 appear to possess an extraordinarily fast wind, but Grauer and Bond (1984) show it to be a fast, multiperiodic variable, with a dominant period of 28.3 minutes and an amplitude of about 0.02 mag. It is identified with the PG 1159 stars (Sion, Liebert, and Starrfield 1985; Starrfield *et al.* 1985). These are located in one (or more) hot instability strips on the $\log L - \log T$ plane, identified by Starrfield *et al.* (1983, 1984). Our color temperature (refer to § IVd and Table 2) of between 150,000 K and 370,000 K places the star in this expected zone.

It is therefore most interesting to note that K1-16 is the only star to show fluxes from various exposures that differ from one another by amounts well outside the expected random variations; see the chronological flux listing in Table 4. Those made during a common shift are enclosed in braces. The largest discrepancy is between SWP exposures 2 and 4, which show a difference of 0.3 mag at 1500 Å. More significantly, we see a drop of 0.18 mag between SWP exposures 3 and 4, which were taken during the same shift (the phenomenon is shown in Fig. 4, which displays SWP exposures 1 and 4). However, a series of successive 10 minute exposures (the last four) exhibit no significant variation. As a comparison, the maximum difference between exposures for any other reliably observed star is 0.13 mag at 1500 Å (for A78). It is 0.10 mag for LoTr-5, and only 0.035 and 0.03 mag for A31 and IC 5148–5150 respectively.

We are not yet certain whether this behavior is related to the optical variability or is only an observational artifact. The lowest fluxes occur for the longest exposure, which was heavily saturated at the shortest wavelengths. This exposure was off center relative to geocoronal Lyman- α , so that an edge effect might be involved. However, SWP exposures 1 and 5, which

PLATE 14

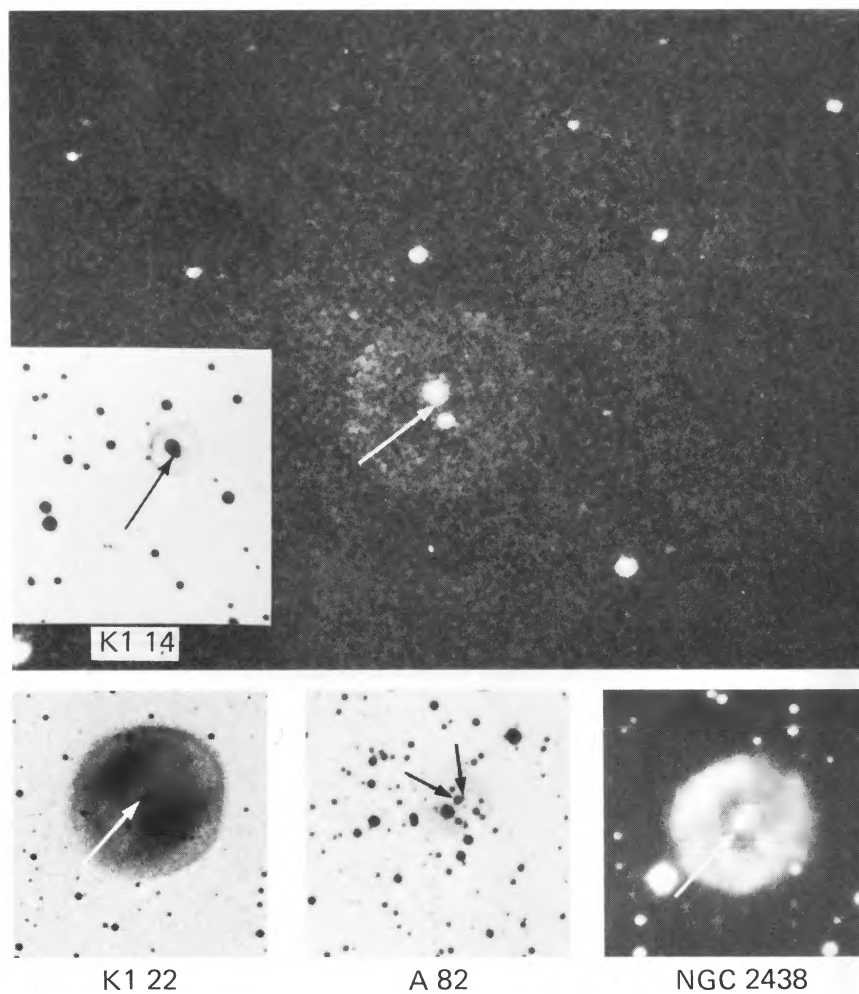


FIG. 10.—Photographs of K1-14, K1-22, A82, and NGC 2438. Two images are presented for K1-14: a larger scale H α photo taken by F. Sabbadin with the 182 cm Asiago reflector, and a smaller scale inset from the blue POSS print. The arrow in the inset points to our initial candidate for the nucleus, and that in the larger photo to the true central star identified by Sabbadin and our *IUE* measurements. Our candidate for the true nucleus of K1-22 is indicated by the arrow. Smith and Gull (1975), however, suggest that the brightest of the trio at the center of K1-22 is the nucleus. The true central star of A82 is unidentified. The arrows point to the bright K star previously thought to be the nucleus and to the star discussed in the text. NGC 2438, whose nucleus also has a neighbor, is shown for comparison and to illustrate the difficulty involved in an optical magnitude measurement. The true nucleus has been known for over 60 yr. The photo of A82 is enlarged from the blue POSS print, © National Geographic-Palomar Observatory Sky Survey, reproduced by permission of the California Institute of Technology; that of K1-22 is taken from the *J* print of the ESO/SRC Survey; NGC 2438 is taken from Curtis (1918).

KALER AND FEIBELMAN (*see page 737*)

appear well centered, still differ by 0.2 mag at 1300 Å. Further observation is mandatory.

d) Color Temperatures

The traditional manner of determining stellar temperatures is through the Zanstra method. The nebular recombination flux is used to infer the integrated stellar flux shortward of the Lyman limit, and its ratio to the flux in the visible yields a kind of broad-band color temperature T_z based on comparison with blackbodies or models.

At the temperatures considered here, generally around 10^5 K, the energy distribution in the optical is quite insensitive to temperature changes; that is, the optical spectrum is very nearly on the Rayleigh-Jeans tail of the blackbody curve. But once we move into the shorter UV wavelengths observed with the *IUE*, we are no longer so restricted. Here, the spectrum displays sufficient sensitivity to allow us to determine color temperatures T_c through the slope of the UV flux curve alone or by comparison of the UV with the optical magnitudes.

An early attempt at deriving T_c was made by Pottasch *et al.* (1978), who used low resolution data from the ANS satellite. They found that the T_c were commonly larger than T_z . However, these data clearly contain systematic errors such that their observed UV slopes were too steep, sometimes considerably beyond an infinite-temperature blackbody. A particular case in point is A78, which they relate to a 140,000 K blackbody, as compared with KFI's likely range of 78,000–84,000 K from the *IUE*. From the *IUE*, Adams and Barlow (1983) found gross inconsistencies between T_c and T_z , whereas Clegg and Seaton (1983) indicated no conflict. Pottasch (1984) also presents T_c from *IUE* data for a number of cooler stars (by planetary standards), as well as for some considered here.

The derivation of T_c for the class of stars we are studying, with $T_z \approx 10^5$ K, has been criticized for the stated reason that the flux curve is too insensitive to temperature for the precision of the *IUE*. Quantitative assessment, however, shows that this opinion is not correct. With careful photometry and correction for interstellar extinction, KFI were able to fit the flux distribution of A78 between 1250 and 6600 Å to a blackbody with an average precision of $\pm 2.9\%$. We cannot do quite as well here under survey conditions, since we generally have fewer exposures per star, observations that are often less than optimal, and fewer UV and optical flux points. Still, in § IIIb we found the mean internal error to be applied to a single flux point to be $\pm 4\%$. The flux ratios, from which values of T_c are found, will be somewhat higher because the errors will be compounded. If we assume a specific model, for now a blackbody, a precision of $\pm 5\%$ (see below) translates into an error of $\pm 20\%$ in T_c at 10^5 K. And even if systematic errors negate an evaluation of *absolute* T_c to that precision, the *IUE* fluxes still allow highly effective *relative* determination. We thus have, at least in principle, a means of evaluating T_z and of finding temperatures of those stars for which the T_z are lower limits.

We effect this temperature analysis by calculating three ratios, or indices, from the fluxes of Table 4 and from the *V* magnitudes of Table 5: $F(\lambda 1300)/F(\lambda 1750)$, $F(\lambda 1500)/F(\lambda 1850)$, and $F(\lambda 1500)/F(V = 5480 \text{ Å})$; these will hereafter be referred to by the ratio of wavelengths, e.g., $\lambda 1500/\lambda 1850$. We give them, corrected for reddening, in columns (2), (3), and (4) of Table 7, including the $\lambda 1500/V$ values from photographic magnitudes. For multiply observed stars, the values given are averages of the ratios found from individual exposures, weighted again according to exposure time (see § IVc), again with the excep-

tion of K1-16, for which we use a straight mean. The 5480 Å fluxes are calculated from *V*, again using the Oke and Schild (1970) calibration. They are corrected for reddening with the extinctions in Table 5, and again the combined SM-Whitford extinction; the Δf_λ are given in footnote a of Table 7 for each ratio. For both A33 and A65 we give the analysis both for the *B–V* extinction, and for the lower values found from nebular photometry.

i) Errors

It is very important that we attempt to derive realistic errors to the indices so that we can evaluate the reality of the derived temperatures. We proceed as for our calculation of the errors to the absolute fluxes in § IIIb and employ stars with multiple exposures, excluding again A28, K1-16, and Sp-1. From comparison of all three ratios, we find that the average mean error for a single ratio is $\pm 5.5\%$; this figure is just what we would expect by compounding the $\pm 3.9\%$ error of the individual fluxes. From the above error and our exposures of Sp-1, we adopt a typical error of $\pm 12\%$ for the underexposed spectra of A28, A43, K1-14, and K3-27, and $\pm 15\%$ for K1-22 (see § IIIb). We arbitrarily assume $\pm 20\%$ errors for the exposure of A82. The final errors that we apply to the corrected ratios are a result of quadratically compounding the errors on the uncorrected ratios (for single exposures the above mean error for a single ratio, and for multiple exposures the mean error calculated from two or more ratios) and the errors in *c* and *V* from Table 5.

There are four sources of systematic error to consider. First, our adopted reddening function may be incorrect or may even vary from one object to another. We have no means of estimating this effect except through the consistency between $c(\lambda 2200)$ and $c(\text{other})$ demonstrated in Table 6, and we simply assume that the error is zero.

Second, we must consider variations in the sensitivity of the spectrograph detectors as a function of wavelength, exposure time, and age. The detectors are clearly changing and becoming less sensitive, so that relative to the calibrations used in the reduction, we will systematically underestimate fluxes as time advances. Sonneborn (1984) shows an average decay for the SWP camera of roughly $1\% \text{ yr}^{-1}$. Our data were acquired over a 3 yr period, so that errors will be made in comparing stars observed at the beginning with those observed at the end; over our interval, the average decay is roughly 2% in sensitivity. It is greatest in the 1225–1375 Å band (3.5% degradation over our observing interval) and least in the 1475–1625 Å band (1%).

We may possibly see this effect in the comparison of multiple exposures in Table 5 in which the fluxes are presented chronologically for a given star. In most cases, the second measurement, often taken a year or more later, is the lower. However, the later exposures are usually the shorter as well, and thus sensitivity degradation cannot be separated from calibration errors that may cause flux to be a function of exposure time; note that the later 90 minute exposure of A31 does not exhibit this decay. Note also that the severely underexposed spectral images are sometimes related to extreme values of the indices, as for K1-14 and K1-22. In addition, the exposures were made under all kinds of observing conditions, from very quiet US 1 shifts to very noisy US 2, in which we were limited to exposures of under 0.5 hr.

In principle, we could still correct for the effect of sensitivity decay. But we do not know whether the broad-band decay

TABLE 7
 ULTRAVIOLET COLOR TEMPERATURES

Star	Corrected Indices ^a			10 ⁻³ T _c			10 ⁻³ <T _c > ^d adopted	10 ⁻³ T _c SWP/LWR	10 ⁻³ <T _c > ^e FBB	10 ⁻³ T _c (He II)	Notes
	$\frac{\lambda 1300^b}{\lambda 1750}$	$\frac{\lambda 1500}{\lambda 1850}$	$\frac{\lambda 1500}{V}$	$\frac{\lambda 1300}{\lambda 1750}$	$\frac{\lambda 1500}{\lambda 1850}$	$\frac{\lambda 1500}{V}$					
(1)	(2)	(3)	(4)	(5)	(6)	(7)	(8)	(9)	(10)	(11)	(12)
NGC 246	3.17 ^{+0.19}	2.22 ^{+0.05}	147 ⁺¹⁰	430 ^{+∞} -270	240 ⁺²⁶⁰ -80	193 ⁺¹⁰⁰ -50	290 ⁺⁷⁰ -130	300 ⁺¹⁰⁰	137 ^{+35a}	85 ⁺² (H)	
NGC 2438	430 ^{+∞} -330	200 ⁺³⁰⁰ -96	160 ⁺¹²⁵ -50	260 ⁺⁸⁵ -150	275 ⁺¹¹⁰	109 ^{+36a}	147 ⁺⁸	1
NGC 2474-5	3.45 ^{+0.25} -0.19	2.41 ^{+0.13}	145 ⁺⁷⁰ -46	∞	>630	...	∞	...	290 ⁺⁷⁰ -160 265 ⁺⁹⁵ -175	112 ⁺¹⁰	
NGC 2610	2.91 ^{+0.18}	2.108 ^{+0.12}	93 ⁺¹³	132 ⁺¹²⁰ -41	97 ⁺¹⁰⁰ -30	63 ⁺¹⁴ -11	97 ^{+20a}	135 ⁺¹⁰	73 ⁺⁶ -15	100 ⁺² (H)	2
NGC 6058	3.32 ^{+0.19s}	2.27 ^{+0.13}	136 ⁺¹²	86 ⁺¹¹⁴ -23	72 ⁺⁷⁸ -26	53 ⁺¹⁴ -9	70 ^{+10a}	95 ⁺⁶	51 ⁺² -8	69 ⁺¹	
NGC 7008	>320s	>130	140 ⁺⁶⁰ -30	140 ⁺⁶³ -30	141 ⁺¹³	133 ⁺¹⁵ -80	69 ⁺¹	
NGC 7094	2.88 ^{+0.17}	2.13 ^{+0.12}	127 ⁺¹⁰	>320s	>103	108 ⁺⁶² -18	108 ⁺⁶² -18	113 ⁺²⁸	99 ⁺¹⁵ -7	97 ⁺²	3
IC 5148-50	3.43 ^{+0.36} -0.04	2.37 ^{+0.06}	...	∞	∞	...	∞	...	215 ⁺¹⁵ -35 162 ⁺¹⁸ -56	97 ⁺¹⁰	
A15	2.86 ^{+0.17}	2.33 ^{+0.14}	114 ⁺¹⁰	118 ⁺⁷⁸ -33	>180	89 ⁺¹⁸ -15	122 ⁺⁴ -28	185 ⁺⁵⁰	88 ^{+16a}	73 ⁺¹ (H)	
A20	3.03 ^{+0.18}	2.37 ^{+0.13}	143 ⁺¹²	81 ⁺³⁹ -20	>122	76 ⁺¹⁴ -12	88 ⁺³ -8	160 ⁺⁶⁵	65 ^{+16a}	76 ⁺² (H)	
A28	2.83 ^{+0.34}	2.10 ^{+0.25}	50 ⁺¹⁵	195 ⁺⁴⁰⁰ -80	>280	170 ⁺⁹⁰ -45	270 [∞]	...	166 ^{+43a}	98 ⁺² (H)	
A31	3.10 ^{+0.18}	2.34 ^{+0.04}	149 ⁺¹⁰	120 ⁺⁴⁷⁵ -40	>280	132 ⁺¹³⁰ -33	270 [∞]	...	128 ^{+35a}	82 ⁺⁶	4
A33	4.28 ^{+0.25}	2.49 ^{+0.08}	207 ⁺¹⁴	110 ⁺³²⁰ -57	106 ^{+∞} -45	...	108 ⁺² -47	...	66 ⁺² -41 45 ⁺² -30	114 ⁺¹⁹	
A33	3.24 ^{+0.94} -0.18	2.33 ^{+0.16} -0.07	78 ⁺¹⁰² -2	265 ^{+∞} -177	∞	180 ⁺¹⁴⁰ -64	>88X	...	165 ^{+37a}	96 ⁺¹¹	5
A33	3.24 ^{+0.94} -0.18	2.33 ^{+0.16} -0.07	78 ⁺¹⁰² -2	∞	∞	∞	>140X	...	134 ^{+41a}	96 ⁺¹¹	5
A33	3.24 ^{+0.94} -0.18	2.33 ^{+0.16} -0.07	78 ⁺¹⁰² -2	>220	>410	50 ^{+∞} -2	>410	...	>425	95 ⁺¹¹	5
A33	3.24 ^{+0.94} -0.18	2.33 ^{+0.16} -0.07	78 ⁺¹⁰² -2	>160	>410	...	>410	...	>425	95 ⁺¹¹	5

TABLE 7—Continued

Star (1)	Corrected Indices ^a			$10^{-3} T_c$		$10^{-3} \langle T_c \rangle^d$ adopted (8)	$10^{-3} T_c$ SWP/LWR (9)	$10^{-3} \langle T_c \rangle^e$ FBB (10)	$10^{-3} T_z$ (HeII) (11)	Notes (12)
	$\frac{\lambda 1300}{\lambda 1750}$ (2)	$\frac{\lambda 1500}{\lambda 1850}$ (3)	$\frac{\lambda 1500}{V}$ (4)	$\frac{\lambda 1300}{\lambda 1750}$ (5)	$\frac{\lambda 1500}{\lambda 1850}$ (6)					
A34	$3.65 \pm 0.21s$	2.37 ± 0.13	168 ± 14	∞ s	>330	$560^{+\infty}_{-310}$	>330	>270	84 ± 3	
A36	3.20 ± 0.19	2.23 ± 0.12	120 ± 10	∞ s	>300	$560^{+\infty}_{-310}$	>300	>270		
A39	2.45 ± 0.14	2.00 ± 0.11	122 ± 10	$540^{+\infty}_{-360}$	$270^{+\infty}_{-160}$	99^{+23}_{-17}	150λ	105^{+5+22}_{-19}	73 ± 1 (H)	
A43	2.56 ± 0.31	2.05 ± 0.24	78 ± 11	$540^{+\infty}_{-430}$	$270^{+\infty}_{-160}$	84^{+13}_{-12}	104λ	79^{+4+21}_{-19}		
A51	2.93 ± 0.17	2.36 ± 0.13	126 ± 10	60^{+12}_{-8}	75^{+36}_{-19}	101^{+26}_{-15}	$79 \pm 12a$	$69 \pm 20a$	86 ± 2	
A65	5.02 ± 0.29	2.49 ± 0.14	316 ± 26	< 35	54^{+26}_{-x}	87 ± 13	55λ	53λ		
A65	3.29 ± 0.81	2.25 ± 0.16	74^{+82}_{-33}	70^{+51}_{-21}	87^{+0}_{-28}	50^{+10}_{-7}	$69 \pm 11a$	$54 \pm 3^{+6}_{-10}$	68 ± 1 (H)	
A72	2.56 ± 0.15	2.03 ± 0.11	102 ± 9	48^{+34}_{-x}	64^{+0}_{-x}	40^{+8}_{-x}	$51 \pm 7a$	< 40		
A78	2.81 ± 0.09	2.02 ± 0.08	112 ± 8	139^{+130}_{-94}	>260	112^{+28}_{-20}	200λ	$134 \pm 40a$	86 ± 4 (H)	
A82	0.85 ± 0.14	1.62 ± 0.34	33 ± 2	89^{+170}_{-20}	>260	106 ± 26	195λ	$102 \pm 31a$	87 ± 6	6
Jn-1	2.45 ± 0.14	2.16 ± 0.12	33 ± 2	∞	∞	∞	∞	∞	87 ± 6	6
K1-14	1.93 ± 0.25	2.00 ± 0.24	58^{+36}_{-24}	> 80	$340^{+\infty}_{-240}$	47^{+230}_{-x}	$195 \pm 145^{+90}_{-90}$	$98^{+26+200}_{-32}$	87 ± 6	6
K1-16	3.19 ± 0.10	2.26 ± 0.06	150 ± 11	> 57	$340^{+\infty}_{-265}$	37^{+230}_{-x}	$190 \pm 150^{+80}_{-115}$	$68 \pm 15^{+230}_{-23}$	93 ± 3	
				70^{+18}_{-13}	82^{+50}_{-22}	72^{+12}_{-11}	$75 \pm 4^{+9}_{-14}$	$60 \pm 7a$	69 ± 2	
				47^{+16}_{-x}	60^{+30}_{-x}	63 ± 10	$57 \pm 5^{+1}_{-x}$	47λ		
				106^{+24}_{-17}	80^{+24}_{-15}	86^{+13}_{-11}	$90 \pm 8^{+8}_{-16}$	$70 \pm 10a$		
				75^{+17}_{-11}	58^{+26}_{-15}	74^{+10}_{-9}	$69 \pm 6^{+9}_{-4}$	57λ		
				15^{+6}_{-2}	35^{+37}_{-11}	\dots	$25 \pm 10a$	$23 \pm 7a$		7
				60^{+12}_{-8}	$148^{+\infty}_{-63}$	\dots	79λ	$64 \pm 16a$		8
				40^{+10}_{-x}	$100^{+\infty}_{-38}$	\dots	56λ	< 40		
				37^{+9}_{-6}	75^{+225}_{-32}	\dots	$56 \pm 19a$	$42 \pm 10a$		4
				\dots	54^{+250}_{-x}	\dots	\dots	\dots		9
				$500^{+\infty}_{-250}$	$410^{+\infty}_{-210}$	210^{+140}_{-60}	$370 \pm 85a$	$152 \pm 39a$	80 ± 2 (H)	10
				$490^{+\infty}_{-240}$	$410^{+\infty}_{-260}$	200^{+155}_{-115}	$370 \pm 85a$	$130 \pm 50a$		

TABLE 7—Continued

Star	Corrected Indices ^a				10 ⁻³ T _c			10 ⁻³ <T _c > ^d adopted	10 ⁻³ T _c SNP/LWR	10 ⁻³ <T _c > ^e FBB	10 ⁻³ T _z (He II)	Notes
	λ1750 λ1750	λ1500 λ1850	λ1500 V	λ1300 λ1750	λ1500 λ1850	λ1500 V	(6)					
K1-22	4.24 ^{+1.67} -1.41	3.24 ^{+0.54}	212 ⁺⁴²⁰ -150	>110	∞	∞	∞	∞	∞	∞	<125	11
K1-27	2.97 ^{+0.32} -0.16	2.23 ^{+0.13}	...	160 ⁺ -54	270 ⁺ -165	...	220 ⁺⁶⁰ -115	∞	∞	88 ⁺¹⁰ -24	...	
K3-27	2.92 ^{+0.36}	2.33 ^{+0.28}	...	96 ⁺ -21	280 ⁺ -200	...	188 ⁺⁹² -110	∞	∞	65 ⁺⁹ -21		
Lo-1	3.02 ^{+0.35} 0.16	2.29 ^{+0.13}	...	138 ⁺ -68	>87	...	138 ⁺ -68	∞	∞	121 ⁺⁴⁹ -61	98 ⁺³ (H)	4, 12
LoTr-5	3.39 ⁺ -0.14	2.35 ^{+0.06}	...	88 ⁺ -40	>64	...	88 ⁺ -40	∞	∞	80 ⁺³⁰ -40		
Sp-1	3.28 ^{+0.41}	3.09 ^{+0.25}	227 ⁺²⁸	190 ⁺ -70	>150	...	190 ⁺ -40	∞	∞	108 ⁺²⁴ -30		
Ym-29	2.75 ^{+0.16}	2.03 ^{+0.11}	117 ⁺¹⁰	112 ⁺ -31	>100	...	112 ⁺ -12	∞	∞	75 ⁺¹⁵ -25		
				∞	∞	...	∞	∞	∞	185 ⁺⁵ -155		
				∞	∞	...	∞	∞	∞	122 ⁺¹⁴ -29		
				>120	∞	...	∞	∞	∞	∞		
				> 82	∞	...	∞	∞	∞	∞		
				94 ⁺³⁸ -22	82 ⁺⁵⁰ -22	94 ⁺²⁰ -16	90 ⁺⁴ -24	∞	∞	72 ^{+13a}	126 ⁺¹³	
				68 ⁺¹⁸	60 ⁺³⁰ -x	80 ⁺¹³ -14	69 ⁺⁶ -3	∞	∞	53 ^{+15a}		

^a Corrected for extinction with the constants of Table 5. The differences in the reddening function Δf_λ for each ratio are: λ1300/λ1750, Δf = 0.39; λ1500/λ1850, Δf = 0.09; λ1500/V (= λ5450), Δf = 1.35.
^b The letters s and S indicate mild and severe saturation at 1300 Å.
^c The letter x assigned as an error denotes indeterminacy. The ∞ symbol denotes a slope at or above the Rayleigh-Jeans limit.
^d Adopted color temperature derived from procedures indicated by the following: Two errors: Straight mean of temperatures derived from individual ratios (cols. [5]–[7]); the first error is the formal mean error, the second set are error limits compatible with those assigned to individual values. Letter a: Straight mean, but average misses one or more limits, so only formal error is given. Letter l: Two error bars in cols. (5)–(7) do not overlap; adopted temperature is that which fits best to error bars, derived by averaging lower limit to highest temperature and upper limit to lowest; for A15, A36, and A51, this value fits within third error bar; for Jn-1 and K1-14, only two values are available. Letter X: One value infinity; a limit based on λ1300/λ1750, compatible with both others, is adopted. T(λ1300/λ1750) not used in average if λ1300 is saturated. T(λ1500/V) not used in average if V is photographic.
^e Temperatures as calculated with the calibration of FBB. Means and errors are calculated as in col. (8), see note d.
 NOTES.—(1) Indices are contaminated by background continuum and are not given. (2) Temperatures and indices may be contaminated by nebular continuum. (3) No indices available because of high reddening. (4) Error on indices assumed to be ± 12%. (5) Upper entries, c = 0.31; lower, c = 0. (6) Upper entries, c = 0.66; lower, c = 19. (7) Not true central star; ± 20% error assumed. (8) Straight average temperature (type "a" of note d) = 104,000 K. (9) T_c (HIM) anomalously low. (10) Indices are straight means from all exposures. (11) Error on indices assumed to be ± 15%. (12) Indices probably include some nebular continuum.

data are applicable to narrow-band fluxes, and from the above argument, the age effect may simply be lost within calibration and ordinary accidental errors. In any case, we allow for it empirically within our assessment of a $\pm 5.5\%$ error for a single observation. We find that we must, however, apply a correction to results derived from the LWR, which we discuss in § IVd(iii) below. Further recalibrations of the SWP range will be treated in § IVd(iv).

Third, we must consider problems with the centering of the star in the aperture. There is evidence that some stars (notably A28 and Jn-1, see § IVc) were observed at the edge. Such a problem is possible for K1-16 as well, as mentioned in § IVc(iv). This placement certainly causes absolute flux errors, but it is uncertain as to whether it will result in errors in the two indices derived strictly from the *IUE*. We do not allow for such an error and only point out the stars that may be affected.

Finally, the fourth source of systematic error involves the stellar energy distributions in the optical from which extinctions are calculated: see § IVa. We have not iterated our calculated extinction for changes in effective filter wavelength brought about by different extinctions and color temperatures. Nor have we changed $(B-V)_0$ to allow for the color temperatures derived below. The general effect of an iteration would be to increase the indices and the resulting temperatures. We feel that any such corrections would be premature and perhaps even erroneous. Since, as we shall see, UV color temperatures do not necessarily reflect effective temperatures, neither may they give us the correct optical slope. More detailed analysis can be done when more optical data are available.

ii) Derivation of Temperature

We derive color temperatures from the three indices from two sets of models that give temperature extremes in order to

provide bracketing values: blackbodies, which give the highest temperatures from a given slope; and high-gravity hydrogen models, which give the lowest. For the latter we use the 200 series sequence of Hummer and Mihalas (1970, hereafter HM) for $\log g = 7$ for $T \geq 90,000$ K, plus models at $\log g = 5.5$, $T = 75,000$ K; $\log g = 5.0$, $T = 50,000$ K. Helium models (Wesemael 1981) give intermediate temperatures; see KFI and Schönberner and Drilling (1984).

We first present our results graphically in Figures 11, 12, and 13 in the form of color-color diagrams in which we respectively plot $\lambda 1300/\lambda 1750$ versus $\lambda 1500/V$, $\lambda 1500/1850$ versus $\lambda 1500/V$, and $\lambda 1500/\lambda 1850$ versus $\lambda 1300/\lambda 1750$. The blackbody and HM-functions are represented by solid and dashed curves, with ticks representing temperatures at 50,000 K, 75,000 K, 100,000 K, 150,000 K, 200,000 K, and (for the blackbody), 500,000 K. Infinite temperature (the Rayleigh-Jeans, hereafter R-J, slope) is indicated by the end of the solid line. Note that at any given position, the HM temperatures are lower than the blackbody, and that the two merge toward the upper end.

We plot the corrected indices from Table 7 on all three graphs. In Figures 11 and 12 we represent the stars with photographic *V* magnitudes as filled symbols. The two stars for which we give a choice of extinctions, A31 and A65, are plotted with special symbols. Note that these are highly placed even at the lower values of *c*. Saturation at 1300 Å is indicated by boxes.

We see in all three figures that the points scatter appropriately around the curves, from roughly 75,000 K (blackbody) to infinity. As expected, the poorest fitting ratios in the first two of these figures include photographic data. In Figures 11 and 12, the points lie systematically above the curves, such that the UV indices are too large for $\lambda 1500/V$. The tendency is toward a superior fit with the HM curve rather than the blackbody. There is, however, a set of points near or under 100,000 K that

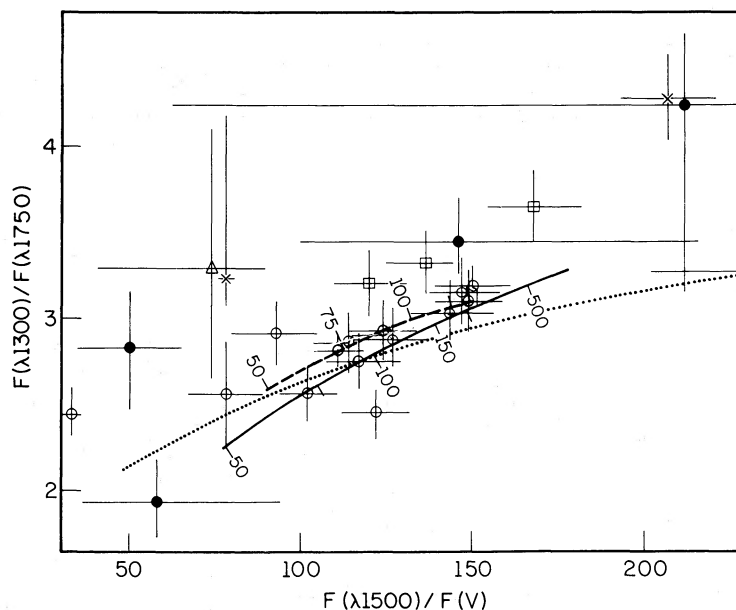


FIG. 11.—The ratio of the flux at 1300 Å to that at 1750 Å plotted against the ratio of the flux at 1500 Å to that at 5480 Å (*V*). The filled symbols are plotted from photographic magnitudes, and are not reliable, as evidenced by large error bars. Two positions, those corresponding to high and low extinctions, are plotted for A33, indicated by crosses. Only the position for the lower extinction is plotted for A65 (triangle); the other is off scale. Squares represent some saturation at 1300 Å. The solid line shows the blackbody locus from 50,000 K to the Rayleigh-Jeans limit; the broken line, the locus for the high-gravity 200 series models by Hummer and Mihalas, from 50,000 K to 200,000 K. The dotted line shows the reddening locus that passes through the 100,000 K blackbody. Ticks are placed on each locus at 50,000 K, 75,000 K, 100,000 K, 150,000 K, 200,000 K, and in the case of the blackbody, at 500,000 K.

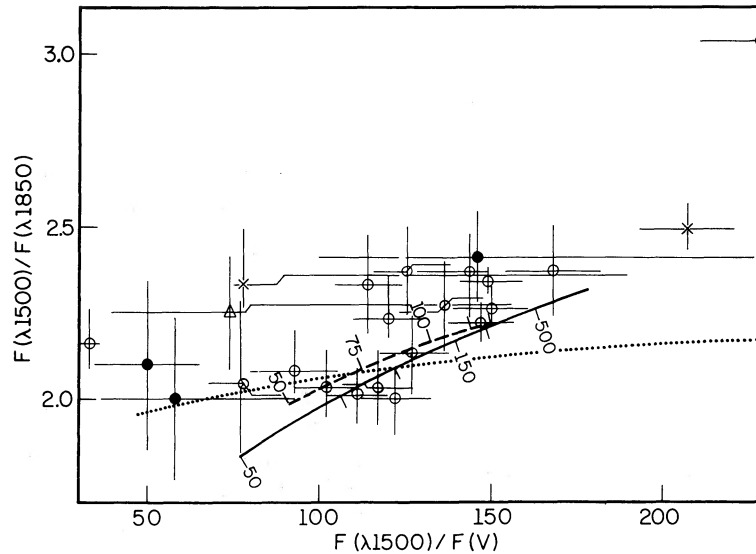


Fig. 12.—Same as Fig. 11, for $\lambda 1500/\lambda 1850$ flux ratio vs. that of $\lambda 1500/\lambda 5480$. K1-22 is off scale.

fits better with the blackbody curve in Figure 12 and with the HM curve in Figure 11. Such discriminations are likely to be spurious given the systematic errors of the *IUE* relative to the visual. The fit around the curves is best for Figure 13, in which only relative *IUE* errors are important.

The scatter in these figures is clearly not produced by errors in the extinctions. The dotted lines in each represent the reddening curves that pass through the 100,000 K blackbody and that do not at all represent the point distribution. Also, the extinctions are generally low, and three of the points at the upper extreme limit have $c = 0$.

Once a model is adopted, we see from the error bars on the

indices that color temperature discrimination is easily possible up to high values, with, of course, a rapidly increasing error as T_c climbs. We also note that *there is no evidence for superinfinite temperatures*, i.e., slopes greater than R-J, as found earlier (see above). The points scatter beyond infinite temperature roughly in accord with their error bars. It is apparent, however, that some of the color temperatures are *close to infinity* in this region of the spectrum, whatever the true effective temperatures might be, at least for the nominal instrumental calibration. High values of this sort have also been noted by Cerruti-Sola *et al.* (1983).

We give the individual color temperatures derived from each

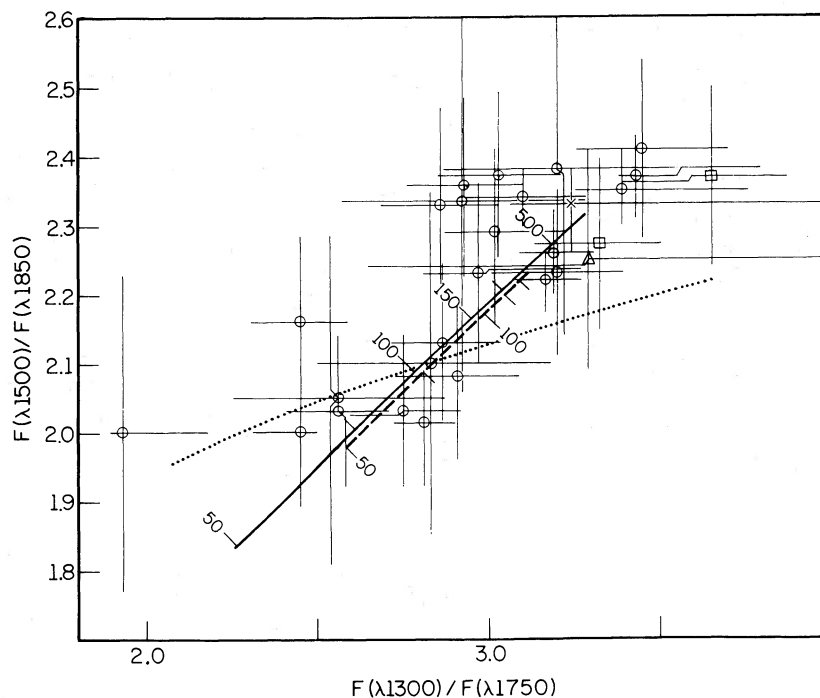


FIG. 13.—Same as Figs. 11 and 12, for the UV flux ratios $\lambda 1500/\lambda 1850$ and $\lambda 1300/\lambda 1750$. A33 and A65 are plotted for the lower extinctions only; the points for the higher extinctions are off scale, as are those that represent Sp-1 and K1-22. Squares again indicate minor saturation at 1300 Å.

of the indices in columns (5), (6), and (7) of Table 7, together with the propagated errors. The first row for each nebula gives T_c found from the Planck function, and the second, that derived from the high-gravity HM models. We give $T_c(\lambda 1500/V)$ only for stars with photoelectric magnitudes, excluding the anomalous Jn-1. For the majority of stars, the three values are reasonably similar, consistent with their placements on Figures 11–13.

If the formal lower limit to an index is greater than the R-J slope, we assign an infinity symbol to the temperature; if the index is larger than R-J but the limit is under, we give a lower limit to T_c . These “infinite” values, as we pointed out above, are most likely simply the result of the scattering of the points just beyond the theoretical limits and of an underestimate of the true error (combined with possible calibration errors; see § IVd[iv]). We do not yet know just how close the slopes actually get to the R-J limit.

Although the scatter is large, the T_c derived from the two UV indices, $\lambda 1300/\lambda 1750$ and $\lambda 1500/\lambda 1850$, on the average agree: in a plot of one versus the other, the points scatter about the 45° line much as they do about the model curves in Figure 13. Also consistent with the color-color plots, the $T_c(\lambda 1500/V)$ are systematically low, with somewhat better overall agreement for the HM models. If we look more closely at details and confine a comparison to $T_c < 100,000$ K, the agreement between $T_c(\lambda 1500/V)$ and $T_c(\lambda 1500/\lambda 1850)$ and between $T_c(\lambda 1500/V)$ and $T_c(\lambda 1300/\lambda 1750)$ is respectively better for blackbodies and for the HM assumption. This difference was commented on above and can be seen in the clustering of points in Figures 11 and 12 about either the blackbody or HM curves. This effect is again probably simply the result of an ultraviolet-to-visual calibration error.

In column (8) we present adopted mean color temperatures $\langle T_c \rangle$ that best represent the two or three individual values in columns (5)–(7). We compute the adopted $\langle T_c \rangle$ in different ways that depend on the sizes of the errors associated with the individual values in column (5)–(7). If the straight mean is consistent with all these errors, it is given in column (8). Two kinds of errors are assigned to these values: the first is the formal mean error, and the second is that range of error that is consistent with the errors attached to the individual values. For the stars marked “a,” the individual T_c are reasonably close to one another, but the average misses one or more of the individual error bars, and the second of the above errors cannot be given. For the stars marked “l,” the individual errors are again inconsistent, the spread is larger, and at least two error bars do not overlap. In this case we adopt a value that is most consistent with the individual errors by averaging the lower limit to the highest value and the upper limit to the lowest. For A15, A36, A51, and the HM temperature of A39, $\langle T_c \rangle$ fits within the third error bar. For A31 the $\lambda 1500/\lambda 1850$ ratio is incompatible with that from $\lambda 1500/V$, and we adopt a limit based on the $\lambda 1300/\lambda 1750$ ratio. Finally, for A34, we give only a limit since the ratios are so high, whereas for the lower color temperatures of K1-27, K3-27, and Lo-1 such a limit is expressed by the errors.

Because of the systematic difference between the temperatures based strictly on the UV and those involving the optical, the adopted values of $\langle T_c \rangle$ will in general be systematically higher for the stars without accurate, photoelectric V magnitudes, for which $T_c(\lambda 1500/V)$ is not computed. However, from Table 7 we see that the three values tend to agree at both infinity and when they are all low, so that the problem pertains primarily to intermediate temperatures, particularly for Lo-1

and K1-27, and possibly for A28 and K3-27. *In any case, we present enough data so that the reader is able to make an independent judgment regarding means, adopted values, and errors.*

The mean color temperature from all data for A78 is 87,000 K. This figure compares very well with the value of 84,000 K found from the very detailed fit by KF1 for a similar assumption of extinction (see their Table 4), showing that our simple indices yield consistent results.

iii) SWP-LWR Ratios

So far, we have neglected the LWR region, primarily because these data are nowhere nearly as extensive, and because this wavelength region must be treated differently as the sensitivity to T_c within its confines is significantly lower. In Table 5 we give fluxes at LWR wavelengths that are mated to those in the SWP region through common extinction across the 2200 Å bump. The SWP/LWR indices $\lambda 1300/\lambda 2070$, $\lambda 1300/\lambda 2270$, and $\lambda 1500/2350$ are independent of extinction (based on the SM function) and have the side benefit of a longer wavelength base than the two indices based strictly on the SWP observations.

The problem is that we must compare fluxes from two cameras with different intensity transfer functions and flux calibrations, with a much greater likelihood of serious systematic error (probably greater than the error brought about by comparing the SWP to the visual, since the magnitudes should be quite accurate). Such an error is easily detected, in that the SWP/LWR indices calculated from Table 5 yield T_c values that are significantly above those from the SWP. The culprit appears to be the sensitivity degradation of the LWR camera: Sonneborn’s (1984) measurements show a much larger decay for the $\lambda 2250$ – $\lambda 2550$ band than for any of the SWP regions, some 8% during our observing interval. We correct for this effect by computing the average decay between the relevant LWR and SWP test bands, from the time of Bohlin and Holm’s (1980) recalibration to the midpoint of our observation period. We then find that we must decrease all the SWP/LWR flux ratios on the average by 7%; we do not feel that the data warrant any finer error discrimination at this time.

We present only the final results in column (9) of Table 7. In the case of multiple exposures, we calculate the mean SWP/LWR indices from the mean fluxes (as opposed to the two SWP indices, for which the mean is the average of the individual ratios; as long as we confine ourselves to a single camera, we believe that the latter procedure reduces systematic error). We then divide the result by 1.07 (note here that the fluxes presented in Table 5 are *not* corrected for sensitivity decay). The mean values of T_c in column (10) are the straight averages of the individual T_c found from the three indices. The errors assigned are simply the formal mean errors, since we do not have enough information to provide a more detailed error analysis.

In general, we see good agreement with the adopted $\langle T_c \rangle$ in column (8), although the SWP/LWR temperatures still tend to be high, A36 especially so. If we ignore A36, the ratio of the mean SWP/LWR temperature to $\langle T_c \rangle$ of column (8) is 1.16 ± 0.10 for either model assumption.

iv) SWP Calibration

Here we would like to examine the SWP calibration problem in somewhat more detail. We have used the nominal, standard, *IUE* calibration throughout this discussion, and we must explore the effects of divergences from it on our previous conclusions. Application of the sensitivity degradations measured by Sonneborn (1984) make little difference. Since the

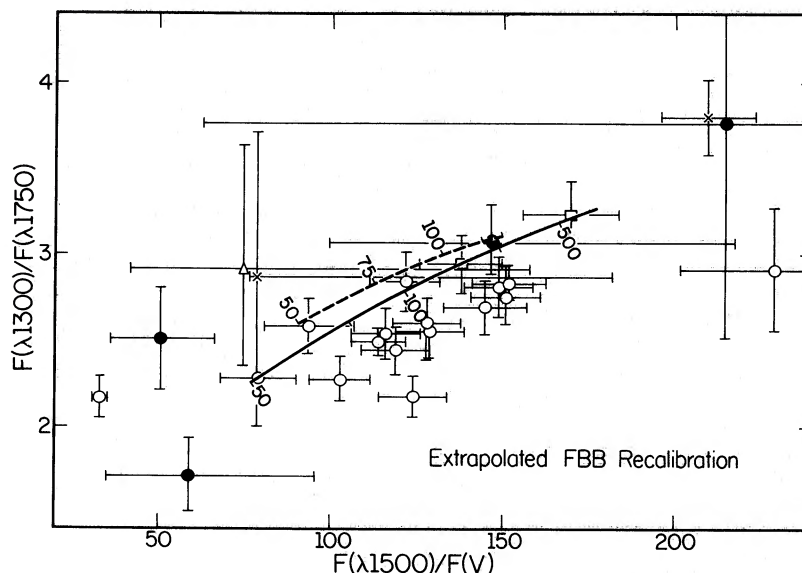


FIG. 14.—Same as Fig. 11, except that the FBB calibration (with our extrapolation to 1300 Å) is used to derive $\langle T_c \rangle$

greatest change is seen for the 1225–1375 Å band, the indices and temperatures actually increase slightly, and in the case of the $\lambda 1300/\lambda 1750$ – $\lambda 1500/V$ plot, the fit gets noticeably worse.

Finley, Basri, and Bowyer (1984, hereafter FBB) have recalibrated nearly the entire *IUE* range through a comparison of observations of white dwarfs with theoretical models based on optically derived temperatures. We use the mean of their curves for 1981 and 1982. The 1300 Å correction is uncertain, since FBB supply data only longward of 1320 Å, and we extrapolated to our shortest wavelength so as to produce an extreme correction. From this recalibration curve, we find that we must, on the average, multiply our $\lambda 1300/\lambda 1750$, $\lambda 1500/\lambda 1850$, and $\lambda 1500/V$ indices by 0.888, 0.935, and 1.014 respectively. We present the recalibrated distribution of points in Figures 14, 15, and 16 respectively. The effect is to slide the

points down the curves to significantly lower temperatures. Although there is still a large range, the points (especially for the $\lambda 1300/\lambda 1750$ – $\lambda 1500/\lambda 1850$ plot) now fall noticeably below the R-J limit. We present the mean color temperatures $\langle T_c \rangle$ (FBB), calculated just as before, in column (10) of Table 7.

We can evaluate this modified FBB calibration empirically. First, it does not compare well with Sonneborn's (1984) measurements: the FBB curve with any reasonable extrapolation shows an increase in $\lambda 1300/\lambda 1750$, whereas Sonneborn indicates a *decrease* of about 4%. Second, the fits between our data and the expected blackbody–HM functions is not as good after recalibration, as seen from inspection of the paired Figures 11–14, 12–15, and 13–16. The points in Figure 14 now fall distinctly under the curve; the fits in Figures 12 and 15 are similar, just switched from above to below; and in the recalib-

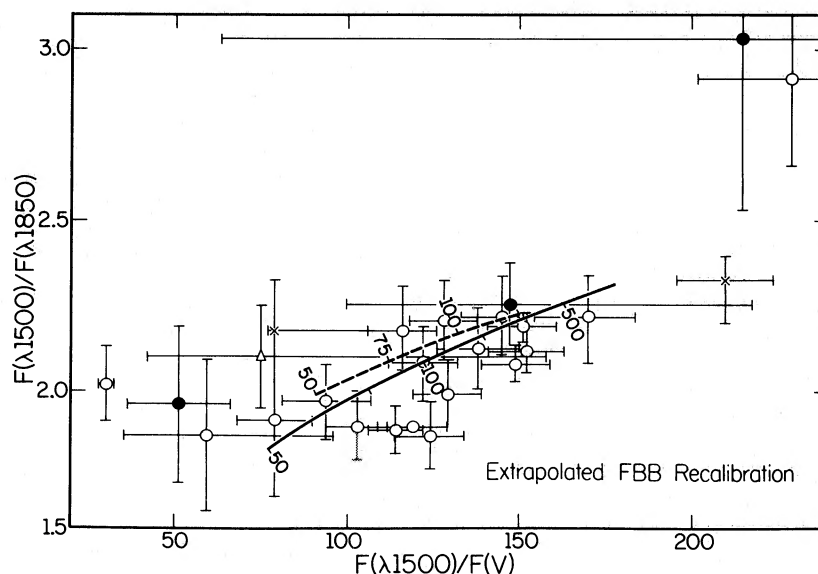


FIG. 15.—Same as Fig. 12, except that our modified FBB calibration is used to derive $\langle T_c \rangle$

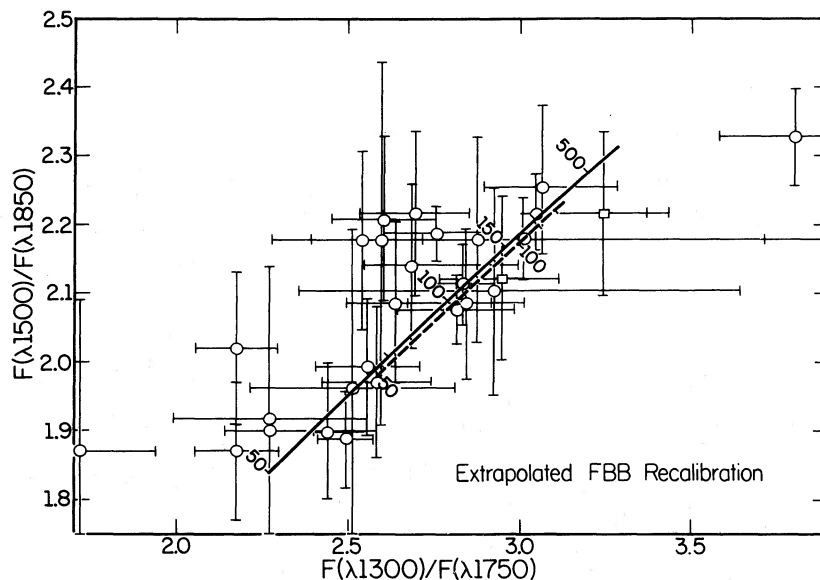


FIG. 16.—Same as Fig. 13, except that our modified FBB calibration is used to derive $\langle T_c \rangle$.

rated plot showing only the *IUE* ratios, the points clearly fall above the line. However, this second argument is much weakened if we extrapolate to a higher correction at $\lambda 1300$.

Third, we also tested our modified FBB calibration by correcting the data that we used in our analysis of A78 (see KF1). With the recalibration applied to our standard star (NGC 7094), the agreement in the extinctions calculated from our three chosen wavelength intervals is much worse; we could not even find a reasonable solution for the 1800–2400 Å interval. If we use the “standard extinction” employed by KF1 and attempt to fit the recalibrated ultraviolet data to the optical (see KF1 Table 4 and the associated text), we cannot find a convergent solution between temperature and extinction. However, fitting and testing over the UV alone between 1250–3000 and 1250–1800 Å (see KF1 Table 5) produces solutions with comparable, actually slightly better, precision near and below the Zanstra temperature (66,000 K and 63,000 K respectively). Although the solutions are accurate, we believe the resulting temperatures to be unrealistic, since because of the very high excitation of the nebula, the effective temperature should be clearly well above 67,000 K.

It is our opinion here from all the above analysis that our modified FBB calibration (including our extrapolation to 1300 Å) overcorrects the data and that the fit of the ultraviolet to the optical becomes poorer. Some recalibration is certainly necessary, and we feel that the temperatures given in columns (8) and (10) of Table 7 represent upper and lower possible extreme values. However, until detailed empirical recalibration can be performed observationally, we will continue to adopt the nominal calibration. Again, we emphasize that sufficient information is given in this paper to allow the reader to apply any recalibrations that may become available.

V. DISCUSSION

What do these color temperatures signify, and how do they relate to one another and to effective and Zanstra temperatures? We can provide only partial answers here. This is the first survey to explore accurately and in depth color tem-

peratures for such hot stars, and there is a great deal of observational work yet to be done.

For purposes of comparison, we must provide Zanstra temperatures, which we give in column (11) of Table 7. These are all blackbody He II temperatures, modified from Kaler (1983a) for the extinctions in Table 5 and for the $V(UV, T_c)$, which we substitute when only visual photographic magnitudes are available. The exception is A28, for which we retain the magnitude estimate from the POSS since we suspect an aperture effect. Of the stars presented, only IC 5148–5150 was not included by Kaler (1983a). For this object, we make use of recent unpublished Kitt Peak IIDS observations, from which we find $I(\lambda 4686)/H\beta \approx 0.5$ and derive an approximate $H\beta$ flux from the $H\beta$ surface brightness. Temperatures that we expect to be lower limits because of high helium ionization (such that the nebulae are optically thin in the He II Lyman continuum) are marked “(H).” Data on He II $\lambda 4686$ are not available for four nebulae (K1-27, Lo-1 = K1-26, LoTr-5, and Sp-1), so that we can calculate only hydrogen Zanstra temperatures. These are inordinately low because of the optically thin nature of these objects, and there is no point in giving them.

We present the distribution of our survey stars on the $\log L - \log T$ plane in Figure 17. The plot is taken directly from Kaler’s (1983a) study of large planetaries. In order that we can see them within the context of the much larger optical data set, our stars are shown by large symbols with their names, where necessary modified in position for the different $T_Z(\text{He II})$ of Table 7. The other stars in Kaler (1983a) are represented by small symbols. The higher of the two extinctions, those from $B - V$, are used for A33 and A65.

Major goals for this work were the testing of Zanstra temperatures for the nebulae thick in the He⁺ Lyman continuum, in order to examine the Zanstra discrepancy (in which the He II temperature is greater than the hydrogen Zanstra temperature; see Kaler 1985a), and determination of temperatures for nebulae that are optically thin, for which the $T_Z(\text{He II})$ values are lower limits. Unfortunately, while the two data sets—UV and optical—are not exactly mutually exclusive,

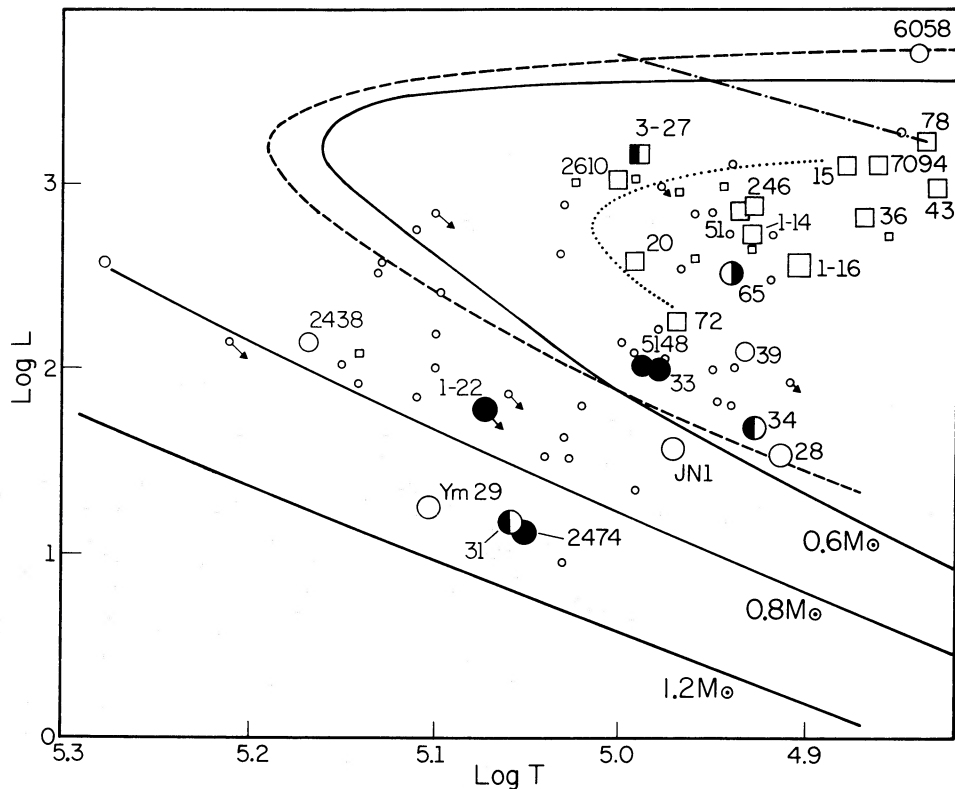


FIG. 17.—The stars on the $\log L$ - $\log T$ plane. The figure is taken from Kaler (1983a), where the points represent the stars placed in that optical study; only IC 5148–5150 has been added. The stars examined in our *IUE* survey are shown as large symbols and are identified by name (usually only catalogue number). Their positions have been modified according to the extinctions and magnitudes used here; the higher values of extinction are used for A33 and A65. *Squares*: stars for which only lower limits are known to T , because the nebula is of high excitation (helium is nearly all doubly ionized) and is optically thin in the He^+ Lyman continuum. The stars should lie along loci parallel to that projecting upward and to the left of A78. *Circles*: nuclei of lower excitation optically thick nebulae, for which the Zanstra temperature should be correct. *Filled symbols*: stars with Rayleigh-Jeans R-J energy distributions. *Half-filled symbols*: stars whose limits allow them to have R-J slopes (see text). The A65 symbol is half-filled oppositely to the others to indicate that its R-J status rests on the higher value of extinction. Note that the filled symbols strongly tend toward lower luminosity. The curves are theoretical evolutionary tracks for stars of different masses. *Solid lines*: Paczyński (1971); *dashed line*: Iben and Renzini (1982); *dotted line*: Schönberner and Weidemann (1981).

there is a distinct systematic selection present. The thin nebulae tend to have luminous nuclei that are easy to observe with the *IUE*, while the thick nebulae tend toward the opposite. Consequently, where we have high-quality UV data, with relatively low errors, we do not have temperature, and where we do have a good temperature, the UV data tend to be much noisier.

The correlation between $\langle T_c \rangle$ and $T_z(\text{He II})$ (shown for the blackbody assumption in Fig. 18, and again assuming our modified FBB calibration in Fig. 19) is frustratingly poor. Although at first glance it looks as if there may be an upper envelope to the distribution (from lower left to upper right), note that the points defining it are lower limits in T_z . We see a similar type of correlation if we plot the $\langle T_c \rangle$ calculated with the HM models against Cahn's (1984) model T_z , so that the problem is not simply a matter of the inapplicability of the blackbody.

One of the primary results of this study is in fact the *lack* of clear correlation; the other is the existence of UV and UV-to-optical flux distributions that are near or at the R-J limit. These two results are, of course, obviously coupled. Together they show us that current models are inadequate; none at present can reproduce the steep UV slopes observed for some stars. Consequently, can we trust their application to other problems involving hot stars, such as the determination of chemical composition?

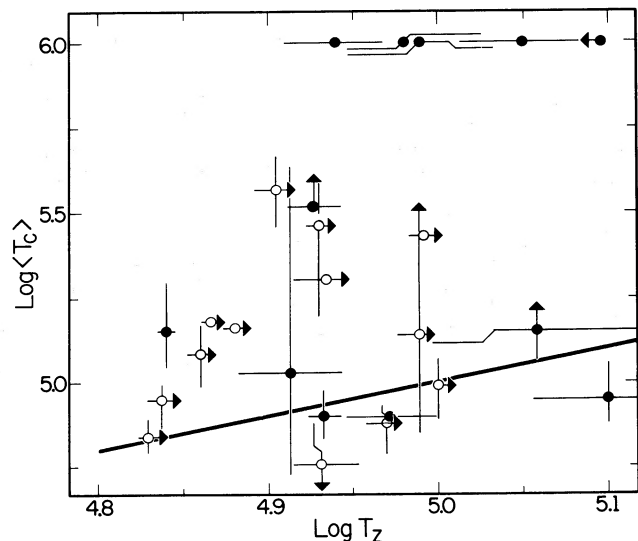


FIG. 18.—A comparison of temperatures, with the mean blackbody ultraviolet color temperatures $\langle T_c \rangle$ from col. (8) of Table 7 (first row for each star) plotted against the He II Zanstra temperatures from col. (11). Lower limits to T_z for stars of high excitation nebulae are indicated by arrows. Stars with R-J continua are arbitrarily set at $\langle \log T_c \rangle = 6.0$. Nuclei of optically thick nebulae are represented by filled symbols. The line represents agreement between the two axes.

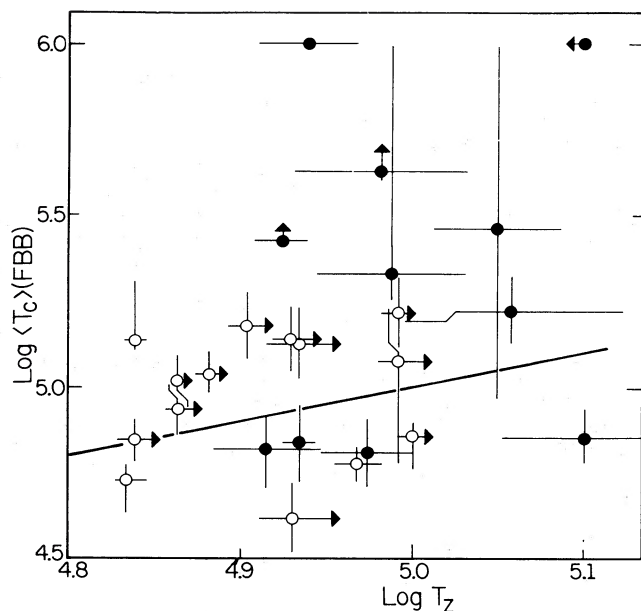


FIG. 19.—The same as Fig. 18 except that our modified FBB recalibration is employed for $\langle T_c \rangle$.

Actually, the data and the plot in Figure 18 do contain a possible correlation. Nuclei of high-excitation nebulae, those with only lower limits to $T_z(\text{He II})$ (among the open circles in the figure), have defined, although perhaps high, color temperatures, below infinity. An exception is K3-27, which has an open upper limit but whose spectrum is probably contaminated. (K1-27 may be another exception, as T_c is compatible with the R-J limit, and Henize and Fairall 1981 show that $\lambda 4686$ is very strong.) The stars with R-J slopes are those involved with lower excitation thick nebulae, represented by the filled symbols. We must point out that the placement of A65 is debatable (due to an uncertain extinction), but also note that A31 and A34, both lower excitation nebulae, have nuclei measured at the R-J limit, though their adopted errors take them to lower, definable T_c (where they are placed in Fig. 15). In addition, $T_c = \infty$ for LoTr-5; even though the nebula does not have a determination of optical depth, from its size (see Feibelman and Kaler 1983; Kaler 1983a), it is likely to be thick in He^+ . Not all the thick, lower excitation nebulae have stars with R-J slopes; some have low, well-defined temperatures. But of these, A28 and possibly Jn-1 suffer from edge effects and the $\langle T_c \rangle$ may not be reliable.

The correlation is also easily seen on the $\log L - \log T$ plane in Figure 17, in which we now fill in the symbols representing the R-J stars. The four with uncertain flux distributions discussed above (A31, A34, A65, and K3-27) we represent by half-filled symbols. The symbol for A33 is filled in spite of the two sets of results given, since we consider the $B - V$ extinction used here to be more secure than it is for A65. Again, the correlation discussed above is clear: the stars with $\langle T_c \rangle = \infty$ fall also toward lower luminosity, generally below $\log L/L_\odot = 2$, in the region of the evolutionary cooling tracks, where the nebulae are thick. Within each group, however, there is no discernible correlation, nor is there a continuous correlation across the total set. What we see is a gross separation; anything finer may simply be masked by errors.

This feature is supported by the work of Schönberner and Drilling (1984), who find that the integrated SWP/LWR flux

ratio is greater than the R-J limit for NGC 7293 and for the sd0 star LSE 21 and is very near the limit for LSS 1362. For their stars, the correction for sensitivity decay from Sonneborn (1984) is more like 3%, which still leaves the first two above the limit and the last at a very high color temperature, around 500,000 K, compatible within a likely error of the R-J limit. NGC 7293 is an optically thick, low-excitation nebula with a low-luminosity star (Kaler 1983a), and the two sd0 stars are among those with the lowest luminosities in their list, quite compatible with the distribution in Fig. 14.

The origin of the problem is unknown, but it is possible that winds and circumstellar matter may be involved. Heap (1982) pointed out that winds are produced by high-luminosity nuclei, with $\log L/L_\odot > 3.85$. Taking her lowest observed luminosity and correcting for the distance scale used here, we can lower that limit to $\log L/L_\odot > 3.3$. From our line features in Table 2, we might drop the limit further to $\log L/L_\odot > 2.5$, but only a lower limit is known to the luminosities of the defining stars, A20 and K1-16. But no emission features are observed below $\log L/L_\odot = 2.5$ (although note that selection is again involved, since these are our noisier spectra and wind signatures may be hidden). Thus it is the class of windy, mass-losing stars that have determinable color temperatures. The low-luminosity stars, those that should have far simpler atmospheres and which should be most amenable to modeling, are the ones that sometimes, though by no means always, exhibit the bizarre R-J slopes. A possible exception is A65, which appears to have an R-J slope, and for which there is a weak suggestion of a wind (Table 2). This result is moderated somewhat if the lower FBB recalibration temperatures are adopted (§ IVd[iv]), since except for K1-22, Sp-1, and the higher extinction of A65, all the $\langle T_c \rangle$ are then below the R-J limit.

We suggest from this behavior that while the UV color temperatures may not yield proper effective temperatures, they may provide upper limits, some of which may be close to the truth for windy stars like A78. For the high-excitation nebulae, the evidence implies that the effective temperature is bracketed by $T_z(\text{He II})$ and $\langle T_c \rangle$.

The resolution of the Zanstra discrepancy is complicated by the *IUE* calibration problem. In Figure 18 (which uses the normal calibration), the line of agreement acts as a general lower limit to the point distributions, implying that the $T_z(\text{He II})$ are a reasonable measure of effective temperature. The stars near the line then provide a calibration for the *IUE* that makes the higher indices and temperatures more credible. But if we go to our extreme recalibration from FBB (Fig. 19), we see that numerous points drop significantly below the line, i.e., $\langle T_c \rangle < T_z(\text{He II})$, suggesting the possibility of the He II excess discussed elsewhere by, for example, Adam and Köppen (1985) and Husfeld *et al.* (1984). Given our opinion that the standard calibration is superior, we suggest that, at least for these kinds of large nebulae, the Zanstra discrepancy is simply resolved by arguments of optical depth, as discussed by Kaler (1983a).

Hummer (private communication) suggests that the color temperatures may be related to stellar compositions. It would be interesting to see whether T_c correlates with these, either as observed directly or as implied by nebular compositions. However, there are as yet not enough data. Méndez, Kudritzki, and Simon (1985) give helium-to-hydrogen ratios for only six of the stars included here (including NGC 7293 that we include from Schönberner and Drilling 1984, discussed above). It is interesting to note that helium-poor NGC 7293 is near the R-J

limit; that A78, with T_c among the lower values, is helium-rich (as implied by nebular analysis, see Jacoby and Ford 1983); and that some other stars are intermediate in both variables. But the number of data points is clearly insufficient; far more are needed to separate any compositional effects from those that may be produced by winds that may affect stars like A78. We fare no better with the available nebular data. Again, only six of our stars have nebular N/O ratios, from Kaler (1983a, 1985b), and the data are strongly biased toward low-excitation objects with strong [N II] and [O II] lines. We see no correlations: NGC 2474–2475 and Ym-29 both have high N/O, but T_c near the opposite extremes. This whole subject should be pursued vigorously so as to measure nebular and stellar compositions for as many of the stars in this sample as possible.

VI. SUMMARY AND CONCLUSIONS

Our initial survey of the central stars of large planetaries is complete. We have observed 32 nuclei selected from a large sample of nebulae optically studied by Kaler (1983a). The fundamental data consist of the measurement of fluxes at several wavelengths, together with an extensive error analysis that demonstrates the capabilities of the *IUE*.

The most important result of the work has been the derivation of ultraviolet and UV-to-optical flux ratios from which we derive color temperatures. The distribution of these color temperatures ranges from rough agreement with the Zanstra temperatures upward to infinite values, far in excess of those derived from the Zanstra method. We have evidence that some stars have UV flux distributions at or near the R-J limit. Recalibration of the *IUE* may lower these temperatures below the R-J limit, however. We believe our extrapolated FBB recalibration to be too extreme, but even if we adopt it, we see that several stars are extremely hot, still well above their Zanstra temperatures.

We find a gross correlation with luminosity: the high-luminosity stars, those for which only lower limits to Zanstra temperature are known because of low nebular optical depth, have generally lower, determinable, color temperatures; the infinite or indeterminable color temperatures are contained by the set of lower luminosity stars. Winds and circumstellar material may be a factor. The role of atmospheric composition is unclear, largely because of lack of data.

We believe that the color temperatures based on the standard calibration represent upper limits to the effective temperatures. If color and Zanstra temperatures agree, that value probably represents the true effective temperature, and perhaps we can have some confidence in the result. If the color temperature is greater than the Zanstra temperature, and if the latter is derived for an optically thick nebula, the Zanstra value should still be employed as representative of the ionizing ultraviolet. If the nebula is optically thin, the Zanstra temperature is a lower limit, the color temperature an upper limit, and the effective temperature falls somewhere in between. The temperature derived for A78 by KF1 might best be viewed in this manner. We suggest that the Zanstra discrepancy can be resolved for this set of stars by simply invoking nebular optical depth; however, any opinion is dependent on future recalibration of the *IUE*.

Our survey has revealed several other interesting aspects of these stars centered in large, old nebulae, enumerated below.

1. We have identified numerous spectral features, including absorption and emission, and P Cygni lines. In addition to

A78, which has been studied before, Sp-1, NGC 7094, and tentatively K1-16 display P Cygni features that are characteristic of relatively high mass-loss rates. The latter two show C IV, and the first displays O V and N V (with C IV in absorption). We also see that A15 and probably A20 have C IV in emission, also demonstrating mass loss.

2. From the P Cygni profiles we are able to estimate terminal velocities. We adopt 3900 km s^{-1} for A78, which we then apply to NGC 7094, and find a much smaller velocity, $\leq 2000 \text{ km s}^{-1}$, for Sp-1 (from O V). K1-16, if the line is real, has what may be the highest steady wind velocity known, $\sim 8500 \text{ km s}^{-1}$. We find that for these high-temperature stars, v_∞/v_{esc} may be between 4 and 6, suggesting an increase of the ratio with temperature.

3. From the 2200 \AA interstellar feature, we derive extinctions for several stars that agree reasonably well with optical values.

4. From the 1500 \AA fluxes and the color temperatures and reddening constants, we calculate V magnitudes. For more than a third of the set these are the best magnitudes available. For two stars, LoTr-5 and K3-27, accurate values can be determined in no other way because of optical contamination.

5. For K1-14, the UV data provide the correct identification of the central star, and for K1-22 an alternative candidate. For A82, the identification is still obscure.

6. The observations of K1-16 demonstrate a possible UV variation that may be related to the optical oscillation.

7. We establish a luminosity limit to wind production that may be as low as $\log L/L_\odot = 2.5$.

Just as important, this survey provides significant direction for future observational and theoretical studies. We must:

1. Confirm the existence of the Rayleigh-Jeans flux distributions found for several stars;

2. Confirm the reality of marginal lines, e.g., He II $\lambda 1640$ emission in A65;

3. Examine K1-16 to determine whether the observed UV variability is real or an instrumental effect;

4. Improve the precision of measurement so as to find correlations of color temperature with luminosity that may be finer than the bulk relationship demonstrated here;

5. Develop theoretical models that can properly fit the observed spectra;

6. Observe the optical energy distributions of these stars so as to allow for others the detailed comparison with theory made for A78 by KF1;

7. Investigate further the winds of planetary nuclei—in particular, we need to:

a) determine the frequency distribution function of winds;

b) correlate wind phenomena with other stellar parameters;

c) confirm the existence of the extraordinary wind suggested by *IUE* spectra for K1-16, and search for similar stars; and

d) determine more precisely, with high-dispersion spectra, wind velocities and establish velocity gradients;

8. Establish the calibration of the *IUE* as a function of time.

Some of the observational work can and will be done with the *IUE*. But much of it will take the greater light-gathering power and photometric precision of the Space Telescope, for which work of this nature should be a high priority. We cannot properly understand the late stages of stellar evolution and the descent to the white dwarfs, without such extensive and accurate data.

This work was supported by NASA grant NAG 5-171 and NSF grant AST 80-23233, both to the University of Illinois. We would like to thank the *IUE* observatory staff for their indispensable aid; D. Hummer, C. L. Imhoff, R. B. C. Henry, H. Shipman, and S. Starrfield for valuable discussion and com-

mentary; and Craig Stoehr for aid in calculation. We are also grateful to an anonymous referee for excellent suggestions and encouragement, and to Dr. F. Sabbadin for pointing out the correct central star of K1-14 and allowing us to use his photograph.

REFERENCES

- Abbott, D. C. 1978, *Ap. J.*, **225**, 893.
 Abell, G. O. 1966, *Ap. J.*, **144**, 259.
 Acker, A., Gleizes, F., Chopinet, M., Marcout, J., Ochsenbein, F., and Roques, J. M. 1982, *Catalogue of the Central Stars of True and Possible Planetary Nebulae* (Pub. Spéc. du C.D.S., No. 3).
 Adam, J., and Köppen, J. 1985, *Astr. Ap.*, **142**, 461.
 Adams, S., and Barlow, M. J. 1983, *IAU Symposium 103, Planetary Nebulae*, ed. D. Flower (Dordrecht: Reidel), p. 537.
 Allen, C. W. 1973, *Astrophysical Quantities* (Athlone: London).
 Anderson, C. M. 1934, *Lick Obs. Bull.*, **17**, 21.
 Bohlin, R. C., Harrington, J. P., and Stecher, T. P. 1982, *Ap. J.*, **252**, 635.
 Bohlin, R. C., and Holm, A. 1980, *IUE Newsletter*, No. 10, p. 37.
 Cahn, J. H. 1974, *A.J.*, **81**, 407.
 ———. 1984, *Ap. J.*, **279**, 304.
 Cahn, J. H., and Kaler, J. B. 1971, *Ap. J. Suppl.*, **22**, 319.
 Casatella, A., and Barbero, J. 1983, presentation at *IUE Three-Agency Meeting*, March.
 Cerruti-Sola, M., Perinotto, M., Cacciari, C., and Patriarchi, P. 1983, *IAU Symposium 103, Planetary Nebulae*, ed. D. Flower (Dordrecht: Reidel), p. 535.
 Clegg, R. E. S., and Seaton, M. J. 1983, *IAU Symposium 103, Planetary Nebulae*, ed. D. Flower (Dordrecht: Reidel), p. 536.
 Curtis, H. D. 1918, *Lick Obs. Pub.*, **13**, 57.
 Feibelman, W. A., and Kaler, J. B. 1983, *Ap. J.*, **269**, 592.
 Finley, D. S., Basri, G., and Bowyer, S. 1984, in *Future of Ultraviolet Astronomy Based on Six Years of IUE Research*, ed. J. M. Mead, R. D. Chapman, Y. Kondo (NASA Conf. Pub. 2349), p. 277 (FBB).
 Greenstein, J. 1981, *Ap. J.*, **245**, 124.
 Grauer, A. D., and Bond, H. E. 1984, *Ap. J.*, **277**, 211.
 Heap, S. R. 1979, *IAU Symposium 83, Mass Loss and Evolution of O-Type Stars*, eds. P. S. Conti and C. W. H. de Loore, (Dordrecht: Reidel), p. 99.
 ———. 1982, *IAU Symposium 99, Wolf-Rayet Stars: Observations, Physics, Evolution*, ed. C. W. H. de Loore and A. J. Willis (Dordrecht: Reidel), p. 423.
 Henize, K. G., and Fairall, A. P. 1981, *Pub. A.S.P.*, **93**, 435.
 Hummer, D. G., and Mihalas, D. 1970, *JILA Rept.*, No. 101 (HM).
 Husfeld, D., Kudritzki, R. P., Simon, K. P., and Clegg, R. E. S. 1984, *Astr. Ap.*, **134**, 139.
 Iben, I. Jr., and Renzini, A. 1983, *Ann. Rev. Astr. Ap.*, **21**, 271.
 Jacoby, G. H., and Ford, H. A. 1983, *Ap. J.*, **266**, 298.
 Kaler, J. B. 1981, *Ap. J. (Letters)*, **250**, L31.
 ———. 1983a, *Ap. J.*, **271**, 188.
 ———. 1983b, *Ap. J.*, **264**, 594.
 Kaler, J. B. 1985a, *Ann. Rev. Astr. Ap.*, **23**, in press.
 ———. 1985b, *Ap. J.*, **290**, 531.
 Kaler, J. B., and Feibelman, W. A. 1984, *Ap. J.*, **282**, 719 (KF1).
 Kaler, J. B., Mo, J.-E., and Pottasch, S. R. 1985, *Ap. J.*, **288**, 305.
 King, I. R., and Raff, M. I. 1977, *Pub. A.S.P.*, **89**, 120.
 Kohoutek, L. 1971, *Astr. Ap.*, **13**, 493.
 ———. 1977, *Astr. Ap.*, **59**, 137.
 Longmore, A. J. 1977, *M.N.R.A.S.*, **178**, 251.
 Longmore, A. J., and Tritton, S. B. 1980, *M.N.R.A.S.*, **193**, 521.
 Méndez, R. H., Kudritzki, R. P., and Simon, K. P. 1985, *Astr. Ap.*, **142**, 289.
 Moore, C. E. 1971, *Nat. Stand. Ref. Data Service, Nat. Bur. Stand.* **35**, Vol. 1.
 Oke, J. B., and Gunn, J. E. 1983, *Ap. J.*, **266**, 713.
 Oke, J. B., and Schild, R. E. 1970, *Ap. J.*, **161**, 1015.
 Paczyński, B. 1971, *Acta Astr.*, **21**, 417.
 Perek, L., and Kohoutek, L. 1967, *Catalogue of Galactic Planetary Nebulae* (Prague: Czechoslovakian Acad. Sci.) (PK).
 Perinotto, M., Benvenuti, P., and Cerruti-Sola, M. 1982, *Astr. Ap.*, **108**, 314.
 Pottasch, S. R. 1984, *Planetary Nebulae* (Dordrecht: Reidel).
 Pottasch, S. R., Wesselius, P. R., Wu, C.-C., Fieten, H., and van Duinen, P. J. 1978, *Astr. Ap.*, **62**, 95.
 Savage, B. D., and Mathis, J. S. 1979, *Ann. Rev. Astr. Ap.*, **17**, 73 (SM).
 Schönberner, D., and Drilling, J. S. 1984, *Ap. J.*, **278**, 702.
 Schönberner, D., and Weidemann, V. 1981, private communication.
 Seaton, M. J. 1980, *Highlights Astr.*, **5**, 247.
 Shao, C.-Y., and Liller, W. 1973, private communication.
 Shaw, R. A., and Kaler, J. B. 1985, *Ap. J.*, **295**, 537.
 Sion, E. M., Liebert, J., and Starrfield, S. G. 1985, *Ap. J.*, **292**, 471.
 Smith, M. G., and Gull, T. R. 1975, *Astr. Ap.*, **44**, 223.
 Sonneborn, G. 1984, report at *IUE user's meeting*, April.
 Starrfield, S. G., Cox, A. N., Hodson, S. W., and Pesnell, W. D. 1983, *Ap. J. (Letters)*, **268**, L27.
 Starrfield, S. G., Cox, A. N., Kidman, R. B., and Pesnell, W. D. 1984, *Ap. J.*, **281**, 800.
 ———. 1985, *Ap. J. (Letters)*, **293**, L23.
 Stecher, T. P., Maran, S. P., Gull, T. R., Aller, L. H., and Savedoff, M. P. 1982, *Ap. J. (Letters)*, **262**, L41.
 Torres-Peimbert, S., and Peimbert, M. 1978, *Rev. Mexicana Astr. Ap.*, **2**, 181.
 Vorontsov-Velyaminov, B. A. 1961, *Astr. Zh.*, **38**, 75.
 Wesemael, F. 1981, *Ap. J. Suppl.*, **45**, 177.
 Wesemael, F., Auer, L. H., Van Horn, H. M., and Savedoff, F. 1980, *Ap. J. Suppl.*, **43**, 159.
 Whitford, A. E. 1958, *A.J.*, **63**, 201.

WALTER A. FEIBELMAN: Code 684, Laboratory for Astronomy and Solar Physics, NASA/Goddard Space Flight Center, Greenbelt, MD 20771

JAMES B. KALER: University of Illinois, Department of Astronomy, 349 Astronomy Building, 1011 W. Springfield, Urbana, IL 61801